Journal of Building Engineering 73 (2023) 106733

Contents lists available at ScienceDirect

Journal of Building Engineering

journal homepage: www.elsevier.com/locate/jobe

# Exergoeconomic and exergoenvironmental based multi-criteria optimization of a new geothermal district heating system integrated with thermal energy storage driven heat pump

Oguz Arslan [a,*], Asli Ergenekon Arslan [b], Irfan Kurtbas [c]

[a] Mechanical Engineering Department, Engineering Faculty, Bilecik Seyh Edebali University, Bilecik, Turkey
[b] Quality Control in Manufacturing Programme, Vocational School, Bilecik Seyh Edebali University, Bilecik, Turkey
[c] Mechanical Engineering Department, Engineering Faculty, Hitit University, Corum, Turkey

ARTICLE INFO

*Keywords:*
Exergoeconomic analysis
Exergoenvironmental analysis
Geothermal district heating
Multi-criteria decision-making

ABSTRACT

In this study, a new geothermal district heating system, which includes a heat pump (HP) system driven by thermal energy storage (TES) unit, was optimized throughout the multi-criteria decision making analysis named efficiency analysis technique with output satisficing (EATWOS). In this regard, the objective functions were chosen as exergoeconomic and exergoenvironmental indicators varying with the handled designs. 111 different designs formed considering different working parameters and fluids in this aim. Three environment-friendly refrigerants according to their thermal behaviour (wet, dry, and isentropic types) and suitable phase change materials (PCM) according to the design conditions were evaluated. The designed system was evaluated by energy, exergy, exergoeconomic, and exergoenvironmental tools to determine the objective functions. As conclusion, Case 108 with the refrigerant of R1234ze and PCM of RT70HC was determined as the best design. The sustainability index, exergoeconomic factor, exergoenvironmental factor, relative cost, and relative exergoenvironmental impact of this optimal case were determined as 1.24, 0.002583%, 0.0540%, 460.85%, and 649.50%, respectively. For this case, the energy and exergy efficiencies of the system were determined as 74.56% and 19.17%, respectively. In comparison to conventional system, a decrease of 38.86% in relative exergoeconomic cost ($r$) and a decrease of 19.21% in the relative exergoenvironmental impact ($r_b$) were achieved.

## 1. Introduction

Geothermal energy is one of the preferable renewables since it has stable thermodynamic characteristics. This stability is directly pertinent to the reservoir's capacity. So, energy systems based on geothermal sources need to be designed carefully for a sustainable future. The use of geothermal energy is classified as direct use and indirect use [1]. The indirect use includes the conversion of heat energy of the geothermal fluids to a secondary form, such as electricity generation [2]. Energy conversion is not in question in direct use as in balneological use, refrigeration, and heating purposes [3,4]. Amongst the use of geothermal energy, the district heating systems (DHS) take the lead since geothermal energy has considerable potential for this aim [5].

Many researchers handled the geothermal district heating systems (GDHS) to improve the systems. Energy and exergy methods are

* Corresponding author.
*E-mail address:* oguz.arslan@bilecik.edu.tr (O. Arslan).

https://doi.org/10.1016/j.jobe.2023.106733
Received 22 March 2023; Received in revised form 18 April 2023; Accepted 30 April 2023
Available online 5 May 2023

the most used tools to analyze systems. Ozgener et al. [6] comparatively investigated two different GHDSs in Balcova and Salihli provinces. According to the study, the exergy efficiencies were conducted at 42.89 and 59.58% for Balcova and Salihli, respectively. Kecebas et al. [7] investigated the GDHS in the Afyon province. They reported the system's energy and exergy efficiency as 37.59% and 47.54%, respectively. Yazici [8] investigated the renovated GDHS in Afyon province. In the study, the energy and exergy efficiency of the system was reported as 46.17% and 60.63%, respectively. Arslan et al. [9] investigated the GDHS of Simav province. They reported the energy and exergy efficiency of the system as 26.30% and 37.41%, respectively. In a different study for Simav province, Arslan and Arslan [10] investigated the improvement potential of the GDHS based on the Pareto principle. They indicated that it is possible to improve the exergy efficiency of the system by 10.33% in comparison to the current status.

In recent years, studies about the performance improvement of GDHSs were increased. The DHS integrated with heat pump (HP) systems are one of the most common ones in this way [11,12]. Galantino et al. [13] investigated the booster heat pump integration into GDHS for the campus facilities. They indicated that centralized heat pumps significantly improve the performance of the direct use of geothermal resources. Zhang [14] conducted a numerical study for the performance analysis of the GHDS sourced by a ground heat exchanger coupled with a heat pump system. They conducted that it is possible to achieve a coefficient of performance (COP) of approximately 6.7 for the system. Sun et al. [15] investigated a hydrothermal GDHS based on an electric compression HP and a centralized absorption heat transformer. In the study, the HP system was used to reduce the return temperature of the heating network so that the performance of the heat transformer could be increased. The COP and exergy efficiency of the system was reported as 24.5 and 61.4%, respectively. Arat and Arslan [16], in their studies, investigated the a-large-scale heat pump integration into a Simav GDHS. They conducted that the system's best performance was obtained for the refrigerant of R410 with a coefficient of performance (COP) of 9.56 and an exergy efficiency of 76.92%. Economic issues were also handled through a net present value (NPV) analysis in these studies as an objective function for the optimization. The NPV value was determined as 23,195,962 US$. Arat and Arslan [17], in another study, investigated the thermodynamic performance of heat pump integration through neural networks. The results reported the best design characteristics: a COP of 9.66 and an exergy efficiency of 73.4%. The NPV reaches the maximum of 23,463,802 US$. Integrating thermal energy storage (TES) system into DHS is also a practical solution for environmental, economic, and efficiency issues [18–20]. Manente et al. [21] indicated that the TES system integrated into GDHS decreases the consumption of natural gas and electricity. It was reported that a saving of 30% in electricity consumption and 11% in natural gas consumption was available by the TES integration. Arslan and Arslan [22] investigated a residential TES integration into Simav GDHS. Through the system, they conducted an electricity saving of 30.24 GWh and a heat saving of 130.94 GWh per year. The energy and exergy efficiencies of the system were reported as 75.87% and 35.11%, respectively. Also, the study investigated economic issues, and the NPV of the optimal system was 17,860,504 US$. Kyriakis and Younger [23] investigated the integration of the TES system into GDHS to enhance source utilization. In the study, it was aimed to balance the fluctuating demands of the users with a TES unit. It was reported that the levelized cost could be reduced by 15% with an energy efficiency of 87.61%. The coupled use of both TES and HP systems has become widespread in recent years. Kim et al. [24] investigated the operation of the TES system with the geothermal heat pump system (GHPS). The study reported a decrease in operational costs of 36–54%. Hemmatabady et al. [25] investigated boosting the stored geothermal energy by integrating the HP system into DHS with the borehole TES system. In the study, it was reported that it is available to reduce emissions by 60%. In their research, Siddiqui et al. [26] investigated the effects of TES size on DHS including an HP system with TES. The minimum electricity cost was reported for the TES size of 1%. de Araujo Passos et al. [27] investigated the optimization of the minimal HVAC demand. They used a phase change material (PCM) battery for the latent heat storage in the system. They concluded that it was possible to meet the 58% of the annual thermal demand with this passive method. In their previous study, Arslan et al. [28] investigated the TES-based HP integration into GDHS. The study used R600a as the refrigerant and conducted 66 cases considering the different working parameters. They concluded that the HP integration is beneficial from the energy, environmental and economic points of view. The system was found investable with an NPV value of 6.35 million $ and a $CO_2$ reduction of 1435.2 ktons per year for the optimal solution.

The studies mentioned above expose beneficial results from the energy, exergy, emission, and economic points of view. However, all these points were commented on separately for the handling systems. For a sensitive evaluation, the analysis, including the relations between exergy, economics, and environmental aspects, is a need. In this regard, the exergoeconomic and exergoenvironmental analysis are handy tools for evaluating the energy systems since they give critical information about the combined effects of exergy, economics, and environment on the operation and component basis [29]. Mousavi and Mehrpooya [30] evaluated a cascade absorption-compression refrigeration system for low-temperature applications through exergy, exergoeconomic, and exergoenvironmental analysis. They exposed that the outputs of exergoeconomic and exergoenvironmental evaluations are helpful parameters to obtain the effective performance of the handled energy system. Zhang et al. [31] performed exergoeconomic and exergoenvironmental analyses for a novel absorption power cycle driven by geothermal resources. They successfully determined the critical operating factors to improve the system. In another study by Cavalcanti [32], exergoeconomic and exergoenvironmental analyses were successfully conducted for an integrated solar combined power cycle system. The study indicated that the exergoenvironmental analysis was a promising approach for energy conversion systems. In the literature, the exergoeconomic and exergoenvironmental investigations were also successfully conducted for the GDHS. Kecebas and Hepbasli [33] analyzed the geothermal district heating systems through the exergoeconomic method. They indicated that the GDHS would be more beneficial when the heat exchangers are used cost-effectively. The study also indicated that the circulation pumps are the critical components to be improved on a component basis. Kecebas et al. [34], in another study, compared two GDHSs through exergoeconomic analysis. They indicated that the operating costs should be focused on improving the systems since the investment costs do not plan an important role. The GDHS was also investigated through the exergoenvironmental analysis [35,36]. The results showed that the main environmental impact is caused by the operating conditions of GDHS, where the component-related impacts are ignorable. The study shows that the exergy destructions of

the components are the most influential parameter from the environmental point of view. The literature indicates that the combined exergy, economic and environmental analyses give valuable information about the GDHSs under the exergoeconomic and exergoenvironmental factors.

The combined effects of exergetic and economic determinants, exergetic and environmental determinants supply a sensitive decision point at designing stages of the energy systems since it includes the grave to yard effects. The exergoeconomic and exergoenvironmental indicators provide information about the current status of the systems and enable them to draw off a path for improvement. To best knowledge of the authors, there is no optimization study based on the exergoeconomic and exergoenvironmental indicators changing with the design parameters as well as parametric study varying with the design criteria. From this point, this study is the first that offers a guide for the scientific literature. So in this study, a parametric exergoeconomic and exergoenvironmental analysis were conducted for a new geothermal district heating system integrated with a residential HP driven by a TES system. Based on the obtained exergoeconomic and exergoenvironmental indicators, the designed systems were optimized by the multi-criteria decision-making (MCDM) analysis. In this aim, 111 different designs were formed. The most effective design was determined by the efficiency analysis technique with output satisficing (EATWOS).

## 2. Methodology

In this study, the geothermal resources of the Simav province were evaluated for the designed GDHS. Simav geothermal field was located on the southern part of the Simav graben system (39° latitude, 28°.4′ longitude) at Kutahya in the western Anatolia of Turkey. The Simav geothermal field has one re-injection well and eight active production wells with a wellhead temperature ranging between 84 °C and 147 °C and mass flow rate ranging between 35 kg/s and 72 kg/s. The field, with a totally mass flow rate of 462.0 kg/s and a consumable temperature of 133.5 °C, has excellent potential to be evaluated in energy systems for multi-purpose use. However, the resources are just used to heat 5000 residences [10,37]. In this study, a GDHS system boosted by a residential HP system was designed to heat 12500 residences. The GDHS is formed of 5 main structures, namely a geothermal fluid transmission line with a 4250 m length (T-line), heat center (C), district heating transmission line (H-line) with a 4000 m length, residence substation (RS) and heating circuit (HC). The transmission lines are formed pre-insulated geothermal pipes with a diameter of 400 mm and 300 mm for the T-line and H-line, respectively. The heat center is constructed of plate-type heat exchangers (HEx). The HP system includes four components: an evaporator (Eva), condenser (Con), compressor (Comp), and expansion valve (V). The schematic of the system is given in Fig. 1 [28]. The condenser of the HP system was designed as a shell-and-tube type heat exchanger, whereas the evaporator was intended as a latent heat TES system. The TES unit structure is given in Fig. 2 [22].

The evaporator of the HP system was handled as the heat source of the heating circuit for the end use. The heating circuit includes aluminium panel radiators (PR). The designing point was determined considering the peak heat requirements within the values of related standards [38]. So, the heat requirement ($\dot{Q}_{design}$) was determined as 56,130 kW for the district system and 4.5 kW for a single residence [22,39]. In the calculations, the indoor temperature was selected as 22 °C considering the thermal comfort conditions [27].

Three kinds of working fluids were performed considering thermodynamic behaviour. In this aim, the wet type, dry type, and

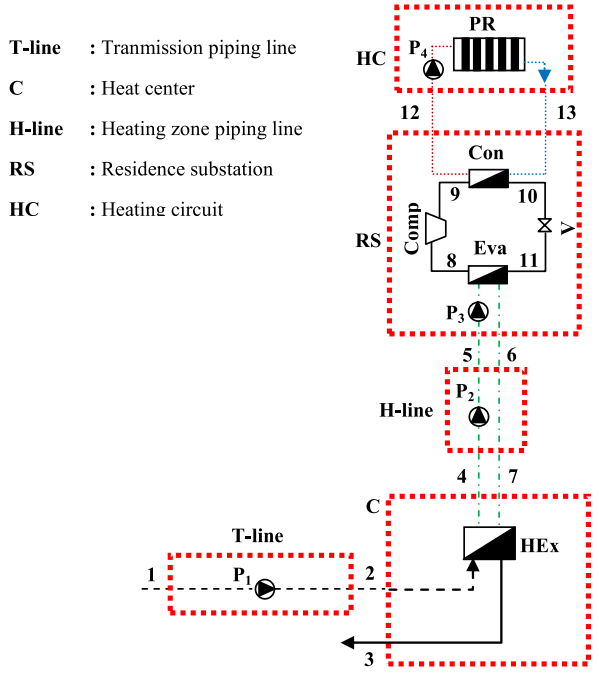


**Fig. 1.** Schematic of GDHS.

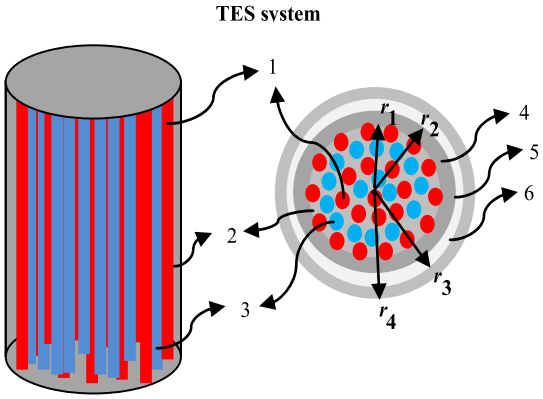


| Component | Explanation | Material | Diameter (mm) | Thickness (mm) | k (W/mK) |
|---|---|---|---|---|---|
| 1 | Heating pipe | St37 | 25 | 4 | 170 |
| 2 | - | PCM | - | - | 0.2 |
| 3 | Cooling pipe | St37 | 25 | 4 | 170 |
| 4 | Shell | St37 | Design parameter | 3 | 170 |
| 5 | Insulation | Rock wool | - | 100 | 0.035 |
| 6 | Cover | Al (Embossed) | Design parameter | 1 | 237 |

**Fig. 2.** Structure of the TES unit [22].

isentropic type fluids were investigated. The working fluids for the HP system were chosen considering the designed working conditions and the temperature scale of the geothermal fluid. The environmental issues, namely ozone depletion potential (ODP) and global warming potential (GWP), were also considered for the selection. In this regard, three working fluids were determined, namely R600a (dry type), R290 (wet type), and R1234ze (isentropic type). The thermophysical properties of the refrigerants were observed from the REFPROP [40]. The properties of used fluids are given in Table 1.

The phase change material (PCM) of the TES system was chosen, taking the appropriate thermal properties for the working conditions (heat capacity, melting temperature, thermal stability, corrosion effects, lower cost, and higher thermal conductivity) into account. With reference to this, organic material namely paraffin wax was used as PCM since it has an unlimited lifetime and it is chemically inert material. The paraffin wax is also high latent heat capacity in the smaller volumes as well as it is quite available to be supplied. The properties of used PCMs are given in Table 2.

### 2.1. Thermal modelling of GDHS components

The Eva was designed as a latent heat-type TES unit with a length ($H$) of 1.5 m according to the typical substation architecture of Simav residences. The TES unit includes St37 pipes ($k_{pipe}$ = 170 W/mK) for charging and discharging (see Fig. 2). The diameter ($D$) of the pipes is 0.025 m with a wall thickness of 0.004 m. The numbers of the required pipes ($n_{pipe}$) and TES volume ($V_{TES}$) in terms of pipe volume ($V_{pipe}$) and PCM volume ($V_{PCM}$) are given by:

$$n_{pipe,charging} = \frac{\dot{Q}_{design}}{\dot{Q}_{pipe,charging}} \tag{1}$$

**Table 1**
Properties of working fluids used in HP system [40–43].

| Properties | R600a | R290 | R1234ze |
|---|---|---|---|
| Fluid characteristic | Dry | Wet | Isentropic |
| Boiling Point (°C) | −11.7 | −42.1 | −18.9 |
| Critical Temperature (°C) | 134.7 | 96.7 | 109.4 |
| Critical Pressure (MPa) | 3.63 | 4.25 | 3.64 |
| Density, $\rho$ (kg/m$^3$)[a] | 508.7 | 436.7 | 1049.6 |
| Dynamic viscosity, $\mu$ (Pa·s)[a] | 0.0083 | 0.0098 | 0.0138 |
| Specific heat, $C_p$ (kJ/kgK)[a] | 2.67 | 3.23 | 1.53 |
| ODP** | 0 | 0 | 0 |
| GWP*** | 4 | 3 | 7 |

[a] Values at 56 °C, ** relative to R11, ***relative to $CO_2$.

**Table 2**
Properties of PCM [44,45].

| Properties | RT55 | RT60 | RT70HC |
|---|---|---|---|
| Density, $\rho$ (kg/m$^3$) | | | |
| Liquid | 770 | 770 | 770 |
| Solid | 880 | 880 | 880 |
| Volumetric expansion, $\beta$ | 1.14 | 1.14 | 1.14 |
| Latent heat capacity (kJ/kg)[a] | 140 | 130 | 230 |
| Conductive heat transfer coefficient, k (W/mK) | 0.2 | 0.2 | 0.2 |
| Dynamic viscosity, $\mu$ (Pa·s) | 0.01 | 0.01 | 0.01 |
| Specific heat, $C_p$ (kJ/kgK) | 2 | 2 | 2 |
| Melting temperature, $T_{melting}$ ($^\circ C$) | 55 | 60 | 70 |

[a] Calculated according to Ref. [44].

$$n_{pipe,discharging} = \frac{\dot{Q}_{design}}{\dot{Q}_{pipe,discharging}} \tag{2}$$

$$V_{TES} = \overbrace{\left(A_{pipe} \bullet \left(n_{pipe,charging} + n_{pipe,discharging}\right) \bullet H\right)}^{V_{pipe}} + \overbrace{\left(\frac{86400 \bullet \left(\dot{Q}_{design} + \dot{Q}_{TES,loss}\right)}{\dot{Q}_{TES}} \bullet \beta\right)}^{V_{PCM}} \tag{3}$$

where $\beta$ is the volumetric expansion coefficient of PCM (see Table 1). The heat transfer rates of charging ($\dot{Q}_{pipe,charging}$) and discharging ($\dot{Q}_{pipe,discharging}$) for a single pipe and heat loss for the total TES volume ($\dot{Q}_{TES,loss}$) are given by:

$$\dot{Q}_{pipe,charging} = \left(\frac{1}{\frac{1}{h_{i,charging}} + \frac{r_i}{k_{pipe}} ln\left(\frac{r_o}{r_i}\right) + \frac{r_o}{r_i}\frac{1}{h_{PCM}}}\right) A_{pipe}\left(\left(\frac{T_5 + T_6}{2}\right) - T_{PCM,melting}\right) \tag{4}$$

$$\dot{Q}_{pipe,discharging} = \left(\frac{1}{\frac{1}{h_{i,discharging}} + \frac{r_i}{k_{pipe}} ln\left(\frac{r_o}{r_i}\right) + \frac{r_o}{r_i}\frac{1}{h_{PCM}}}\right) A_{pipe}\left(T_{PCM,melting} - \left(\frac{T_8 + T_{11}}{2}\right)\right) \tag{5}$$

$$\dot{Q}_{TES,loss} = \left(\frac{1}{\frac{1}{h_{PCM}} + \frac{r_1}{k_4} ln\left(\frac{r_2}{r_1}\right) + \frac{r_1}{k_5} ln\left(\frac{r_3}{r_2}\right) + \frac{r_1}{k_6} ln\left(\frac{r_4}{r_3}\right) + \frac{r_4}{r_1}\frac{1}{h_{ambiance}}}\right) A_{TES}\left(T_{TES} - T_{ambiance}\right) \tag{6}$$

Here, $T_{ambiance}$ was assumed as 10 °C for the substation as the non-heated space with the heat resistance ($1/h_{ambiance}$) of 0.17 m$^2$K/W [38]. $h_{i,charging}$ and $h_{i,discharging}$ are convective heat transfer coefficients of the inner flow. $h_{i,charging}$ was determined considering the laminar flow conditions since all the investigated cases were determined in this manner [46]. $h_{i,discharging}$ was determined considering the boiling process including two terms, namely bubbling boiling heat transfer coefficient ($h_b$) and enforced convective coefficient ($h_e$) [46]. $h_o$ is the convective heat transfer coefficient of the outer flow. Depending on the phase change, it was determined considering the natural convection conditions [47]. These coefficients are given as:

$$h_{i,charging} = \frac{Nu \bullet k_i}{D_i} = \frac{3.66 k_i}{D_i} \tag{7}$$

$$h_{i,discharging} = h_b + h_e$$
$$h_{i,discharging} = \left(0.0122\left(\frac{k_f^{0.79} C_{pf}^{0.45} \rho_f^{0.49}}{\sigma^{0.5} \mu_f^{0.29} h_{fg}^{0.24} \rho_g^{0.24}}\right) \Delta T_s^{0.24} \Delta P_s^{0.75} S\right) + \left(0.023\left(\frac{G(1-x)D}{\mu_f}\right)^{0.8} Pr_f^{0.4} \frac{k_f}{D} F\right) \tag{8}$$

$$h_o = \frac{0.35 \bullet (Gr \bullet Pr)^{0.25}}{\left(1 - \left(\frac{0.143}{Pr}\right)^{\frac{9}{16}}\right)^{\frac{4}{9}}} \frac{k_{PCM}}{D_o} \tag{9}$$

where $D_i$, $D_o$, and $A_{pipe}$ indicate the inner diameter, the outer diameter of the pipe, and the surface area of the pipes, respectively. $T_{PCM,melting}$, $k_i$ and $k_o$ are PCM's melting temperature, the conductive heat transfer coefficients of water and PCM, respectively. $Gr$ and $Pr$ are the Grashof and Prandtl numbers, respectively. Detailed information and validation of the heat transfer model can be achieved from Ref [28]. The Con was modelled as a shell and tube type heat exchanger according to the common use. For the design of 30° triangle

placement, the heat transfer equation in terms of the logarithmic mean temperature ($\Delta T_{lm}$) and correction factor ($F$) is given by Refs. [48,49]:

$$\dot{Q}_{design} = \left( \frac{1}{\frac{1}{h_{tube}} + \frac{ln\left(\frac{D_o}{D_i}\right)}{k_{tube}} + \frac{1}{k_{ins}} ln\left(\frac{r_3}{r_2}\right) + \frac{D_o}{D_i}\frac{1}{h_{shell}}} \right) A_{condenser} \Delta T_{lm} \left( \overbrace{\frac{\sqrt{R^2+1}}{R-1} \frac{ln\left(\frac{1-P}{1-PR}\right)}{ln\left(\frac{2-P\left(R+1-\sqrt{R^2+1}\right)}{2-P\left(R+1+\sqrt{R^2+1}\right)}\right)}}^{F} \right) \tag{10}$$

Here $h_{tube}$ *and* $k_{tube}$ are the inner convective heat transfer coefficient for the condensation process and the conductive heat transfer coefficient of the tube side (Stainless steel-16.3 W/mK), respectively [46]. $h_{shell}$ is the heat transfer coefficient of the shell side [50–52]. $P$ and $R$ are the dimensionless temperature variables. According to the Kern method, the related coefficients are given as [46,48]:

$$h_{tube} = 0.555 \left( \frac{g\rho_f(\rho_f - \rho_g)\left(h_{fg} + 0,375 C_{pf}(T_s - T_w)k_f^3\right)}{\mu_f(T_s - T_w)D} \right)^{0.25} \quad Re_g = \frac{\rho_g V_g D}{\mu_g} < 35000 \tag{11}$$

$$h_{shell} = \frac{Nu \bullet k}{D_e} = \frac{\left(JRe_s\, Pr^{\frac{1}{3}}\left(\frac{\mu}{\mu_w}\right)^{0,14}\right)k}{\frac{4\left(\frac{\sqrt{3}P_t^2}{4}\right) - \frac{\pi D_o^2}{8}}{\frac{\pi D_o}{2}}} = \frac{\left(J\left(\frac{\dot{m}D_e}{\mu(D_s - ND_0)D_s f}\right)Pr^{\frac{1}{3}}\left(\frac{\mu}{\mu_w}\right)^{0,14}\right)k}{\frac{4\left(\frac{\sqrt{3}P_t^2}{4}\right) - \frac{\pi D_o^2}{8}}{\frac{\pi D_o}{2}}} \tag{12}$$

$$\begin{aligned} R &= \frac{T_{12} - T_{13}}{T_9 - T_{10}} \\ P &= \frac{T_9 - T_{10}}{T_9 - T_{13}} \end{aligned} \tag{13}$$

where $J$, $D_s$, $D_e$, $D_o$, $P_t$, and N are the dimensionless heat factor, the inner diameter of the shell side, the equivalent shell diameter, the outer diameter of the tubes, the distance ratio, and the number of central tubes, respectively. $f$ is the baffle cut kept between 0.4 and 0.6 for an effective design [52]. Detailed information can be achieved from Ref. [28]. A titanium-coated plate-type heat exchanger (HEx) with an efficiency of 0.98 was considered to cope with the corrosion and heat loss problems. The required parameters for the modelling are given as [50]:

$$n_{plate} = \frac{A_{HE}}{A_{plate}} \tag{14}$$

$$A_{HE} = \frac{0.98\dot{m}_2(h_2 - h_3)}{\left(\frac{1}{\frac{1}{h_i} + R_i + \frac{l}{k_{plate}} + R_o + \frac{1}{h_o}}\right)\left(\frac{(T_2 - T_4) - (T_3 - T_9)}{ln\left(\frac{T_2 - T_4}{T_3 - T_9}\right)}\right)} \tag{15}$$

where

$$h_{i\ or\ o} = \left( \overbrace{0.2 \bullet Re^{0.67} \bullet Pr^{0.4} \bullet \left(\frac{\mu}{\mu_o}\right)^{0.1}}^{Nu} \right) \frac{k}{D_h} \tag{16}$$

Here $\mu_o$, $D_h$, and $A_{plate}$ indicate the average dynamic viscosity of all streams, the hydraulic diameter (0.0139 m), and the heat transfer area of a single plate (1.38 $m^2$) [53]. The heat losses in the transmission lines were calculated by taking the constant temperature of the soil ($T_{soil}$). In this regard, the related thickness, where the temperature changes occurred by the transferred heat can be neglected, was handled [4,37]. The heat losses in the transmission lines are calculated by:

$$\dot{q}_{loss} = \frac{2\pi(T_i - T_{soil})}{\frac{1}{r_1 h_i} + \frac{1}{k_{pipe}} ln\left(\frac{r_2}{r_1}\right) + \frac{1}{k_{ins}} ln\left(\frac{r_3}{r_2}\right) + \frac{1}{k_{cover}} ln\left(\frac{r_4}{r_3}\right) + \frac{1}{k_{soil}} ln\left(\frac{r_5}{r_4}\right)} \tag{17}$$

With the convective heat transfer coefficient of $h_i$ [46]:

$$h_i = \left( \overbrace{0.012\left(Re_D^{0.8} - 280\right)Pr^{0.4}}^{Nu} \right) \frac{k_{fluid}}{2r_i} \tag{18}$$

where $k_{pipe}$, $k_{ins}$, $k_{cover}$, and $k_{fluid}$ are conductive heat transfer coefficients of the pipe, insulation, cover layers, and working fluid, respectively. Technical properties of the transmission lines are given in Table 3.

The PR was considered in the heating circuit. The panel length with a nominal height of 0.6 m was determined by taking PR's peak heat demand and heating capacity [37].

The required power for the compressor was calculated considering the properties of the fluid at the inlet and outlet conditions. The needed power sourced by the pressure drops of the TES side and cooling pipes side of the Con was also included in the calculations. The required energy for the pumps was calculated considering the pressure drops. In the calculations of the necessary power for the HC pump ($P_4$), the pressure drops of the PR and shell side of the Con were included. In P3, the needed power was calculated considering the heating pipes side of the Con. Assuming the efficiency ($\eta$) of 0.8 for the pumps and compressor, the required power, in terms of the designed conditions of HP and pressure drops ($\Delta P$), is given by:

$$\dot{W}_{pump} = \frac{\dot{m} v \Delta P}{\eta} \tag{19}$$

$$\dot{W}_{compressor} = \frac{\dot{m}((h_9 - h_8) + (v(\Delta P_{Con-side} + \Delta P_{TES-side})))}{\eta} \tag{20}$$

The pressure drop is given as follows:

$$\Delta P = \lambda \frac{L}{D} \frac{\rho V^2}{2} \tag{21}$$

where $L$ and $D$ (or $D_h$) are the length and diameter of the pipes (or plates), respectively. $\lambda$ is the friction factor dependent on Reynolds ($Re$). The friction factors used are given in Table 4.

In terms of dimensionless pressure factor ($J_r$) and the nominal shell diameter ($D_G = 0.19$ m), the pressure drop of the shell side of Con is given by Refs. [28,50,52,54];

$$\Delta P = 8 J_r \frac{D_G}{D_e} \frac{L}{L_b} \frac{\rho V^2}{2} \left(\frac{\mu}{\mu_w}\right)^{-0,14} \tag{22}$$

### 2.2. Energy and exergy analysis

The continuity equation of the $k$th component under steady-state conditions is given by:

$$\sum (\dot{m}_i)_k - \sum (\dot{m}_o)_k = 0 \tag{23}$$

The first law of thermodynamics for the $k$th component under steady-state conditions is given by:

$$\dot{Q}_k - \dot{W}_k + \sum (\dot{m}_i h_i)_k - \sum (\dot{m}_o h_o)_k = 0 \tag{24}$$

The exergy balance of the $k$th component under steady-state conditions is given by:

$$\overbrace{\left(1 - \frac{T_0}{T}\right)\dot{Q}_k}^{\dot{E}x_k^Q} - \overbrace{\dot{W}_k}^{\dot{E}x_k^W} - \sum (\dot{m}_i \psi_i)_k - \sum (\dot{m}_o \psi_o)_k - \dot{E}x_{d,k} = 0 \tag{25}$$

where the specific exergy of a flow ($\psi$) at a particular state is given in terms of enthalpy ($h$) and entropy ($s$):

$$\psi = (h - h_0) - T_0(s - s_0) \tag{26}$$

Here, 0 indicates the reference state conditions taken as 25 °C and 1 atm. $\dot{Q}$, $\dot{W}$, $\dot{E}x_k^Q$, $\dot{E}x_k^W$, and $\dot{E}x_{d,k}$ are the heat rate, work rate, heat exergy, work exergy, and exergy destruction, respectively. The energy and exergy balance equations of the considered system are given in Table 5.

In terms of energy and exergy balances, the efficiency and performance values of the subsystems and overall system are given by:

**Table 3**
Technical characteristics of the transmission lines [9,10].

| Layer | Material | $k$ (W/mK) | $D$ (m) | | | Length-$L$ (m) | |
|---|---|---|---|---|---|---|---|
| | | | H-line | | T-line | H-line | T-line |
| Pipe | St-37 steel | 76 | inner | 0.20 | 0.15 | 4250 | 4000 |
| | | | outer | 0.2063 | 0.1556 | | |
| Insulation | polyurethane | 0.028 | | 0.28 | 0.23 | | |
| Cover | polyethylene | 0.43 | | 0.286 | 0.2352 | | |
| Soil | – | 2.1 | | 0.6 | | | |

**Table 4**
The friction factors for the pumps and compressor.

| Component | | Friction Factor | Explanation | Source |
|---|---|---|---|---|
| T-line pump ($P_1$) | Line side | [a] | – | [55] |
| | HE-1 side | $\lambda = \frac{1.22}{Re^{0.252}}$ | – | [50] |
| H-line pump ($P_2$) | Line side | [a] | – | [55] |
| | HE-1 side | $\lambda = \frac{1.22}{Re^{0.252}}$ | – | [50] |
| Substation pump ($P_3$) | TES side | $\lambda = \frac{64}{Re}$ | $Re < 2300$ | [50] |
| HC pump ($P_4$) | HE-3 side | $\lambda = \frac{15.064}{Re}$ | – | [50] |
| Compressor | TES side | $\lambda = 0.316\left(\frac{1}{Re}\right)^{0.25}$ | $Re < 2\bullet10^4$ | [46] |
| | HE-2 tube side | $\lambda = 0.184\left(\frac{1}{Re}\right)^{0.20}$ | $2\bullet10^4 < Re < 3\bullet10^5$ | |

[a] Taken from Moody diagram.

$$\eta = \frac{\dot{E}_{useful}}{\dot{E}_{in}} \tag{27}$$

$$COP = \frac{\dot{E}_{useful}}{\dot{W}_{in}} \tag{28}$$

$$\varepsilon = 1 - \frac{\dot{E}x_d}{\dot{E}x_{in}} \tag{29}$$

### 2.3. Exergoeconomic analysis

The thermodynamic performance of any energy system is not only the critical parameter, but also the economic outputs are the decisive elements to make a decision for the end users and investors. The exergoeconomic analysis is helpful in this aim since it gives the hybrid results combining the thermodynamic and economic outputs. The exergoeconomic balance of the *k*th component is provided by Ref. [56]:

$$\sum \overbrace{c_{out}\dot{E}x_{out,k}}^{\dot{C}_{out,k}} + \overbrace{c_W\dot{W}_{W,k}}^{\dot{C}_{W,k}} = \sum \overbrace{c_{in}\dot{E}x_{in,k}}^{\dot{C}_{in,k}} + \overbrace{c_Q\dot{E}x_{Q,k}}^{\dot{C}_{Q,k}} + \dot{Z}_k \tag{30}$$

$$\overbrace{c_F\dot{E}x_{F,k}}^{\dot{C}_{F,k}} + \dot{Z}_k = \overbrace{c_P\dot{E}x_{P,k}}^{\dot{C}_{P,k}} \tag{31}$$

where $c$ is the unit cost of exergy flow, and $\dot{C}$ is the exergy cost rate. The subscripts in, out, W, Q, *F,* and *P* indicate the inlet, outlet, work-related term, thermal energy, fuel, and product, respectively. $\dot{Z}$ indicates the investment cost rate of the *k*th component and is given by Ref. [56]:

$$\dot{Z}_k = \dot{Z}_k^{CI} + \dot{Z}_k^{OM} \tag{32}$$

Here, $\dot{Z}_k^{CI}$ and $\dot{Z}_k^{OM}$ indicate the kth component's capital investment and operation and maintenance costs, respectively. In terms of

**Table 5**
Energy and exergy balance equations for GDHS.

| Components | Energy balance | Exergy balance |
|---|---|---|
| T-line | $\dot{Q}_{T-line} = \dot{m}h_2 - \dot{m}h_1 - \dot{W}_{P1}$ | $\dot{E}x_{d,T-line} = (\dot{m}\psi_1 - \dot{m}\psi_2) + \dot{W}_{P1} - \left(1 - \frac{T_0}{T_{ave}}\right)\dot{Q}_{T-line}$ |
| C | $\dot{Q}_C = (\dot{m}h_7 - \dot{m}h_4) - (\dot{m}h_3 - \dot{m}h_2)$ | $\dot{E}x_{d,C} = (\dot{m}\psi_2 + \dot{m}\psi_7) - (\dot{m}\psi_3 + \dot{m}\psi_4) - \left(1 - \frac{T_0}{T_{ave}}\right)\dot{Q}_C$ |
| H-line | $\dot{Q}_{H-line} = (\dot{m}h_5 + \dot{m}h_7) - (\dot{m}h_4 + \dot{m}h_6) - \dot{W}_{P2}$ | $\dot{E}x_{d,H-line} = (\dot{m}\psi_4 + \dot{m}\psi_6) - (\dot{m}\psi_5 + \dot{m}\psi_7) + \dot{W}_{P2} - \left(1 - \frac{T_0}{T_{ave}}\right)\dot{Q}_{H-line}$ |
| HP | $\dot{Q}_{HP} = (\dot{m}h_{12} - \dot{m}h_{13}) - (\dot{m}h_5 - \dot{m}h_6) - \dot{W}_{Comp} - \dot{W}_{P3}$ | $\dot{E}x_{d,HP} = (\dot{m}\psi_5 + \dot{m}\psi_{13}) - (\dot{m}\psi_6 + \dot{m}\psi_{12}) + \dot{W}_{Comp} + \dot{W}_{P3} - \left(1 - \frac{T_0}{T_{ave}}\right)\dot{Q}_{HP}$ |
| HC | $\dot{Q}_{useful} = \dot{m}h_{13} - \dot{m}h_{12} - \dot{W}_{P4}$ | $\dot{E}x_{d,HC} = (\dot{m}\psi_{12} - \dot{m}\psi_{13}) + \dot{W}_{P4} - \left(1 - \frac{T_0}{T_{ave}}\right)\dot{Q}_{useful}$ |
| ***Overall system*** | | $\dot{E}x_{d,total} = \dot{E}x_{d,T-line} + \dot{E}x_{d,C} + \dot{E}x_{d,H-line} + \dot{E}x_{d,HP} + \dot{E}x_{d,HC}$ |

purchasing cost ($Z_0$), operation and maintenance factor ($\varphi$), capital recovery factor ($CRF$), annual operation hours ($N$), and inflation indicator ($InI$), eq. (33) can be written as [56]:

$$\dot{Z}_k = \frac{Z_0 \varphi}{N} \overbrace{\frac{i(1+i)^n}{(1+i)^n - 1}}^{CRF} \overbrace{\frac{CI}{CI_{origin}}}^{InI} \tag{33}$$

In this study, $\varphi$ was taken as 1.06 [57], $N$ was taken as 2683 h [22], $n$ was assumed as 20 years, and inflation rate ($i$) was taken as 15.75% [58]. $InI$ was determined by the ratio of the cost index related to the current year ($CI$) to the reference cost index related to the issued year ($CI_{origin}$) [59]. According to exergoeconomic evaluation, relative cost ($r_k$) and exergoeconomic factor ($f_k$) are the essential parameters for the assessment of the systems [30]. These parameters are given by:

$$r_k = \frac{c_{P,k} - c_{F,k}}{c_{F,k}} \tag{34}$$

$$f_k = \frac{\dot{Z}_k}{\dot{Z}_k + \dot{C}_{d,k}} \tag{35}$$

where $\dot{C}_{d,k}$ is the exergy destruction cost and is defined as [56]:

$$\dot{C}_{d,k} = c_{F,k} \dot{E}x_{d,k} \tag{36}$$

Cost balances and auxiliary equations of the GDHS are given in Table 6, and the cost functions of the components are shown in Table 7.

### 2.4. Exergoenvironmental analysis

Exergoenvironmental analysis is a helpful tool for evaluating the systems and designs since it enables observing how the environmental impacts change through energetic development. Exergoenvironmental analysis is also beneficial since it includes the environmental impacts from production to disposal of any system component as well as the operating effects. In this regard, the life cycle assessment ($LCA$) is an appropriate tool to determine the environmental impacts of any system. An environmental assessment is performed using an indicator [29]. In this study, Eco-indicator 99 method was used for $LCA$ [60]. The component-related environmental impacts in $LCA$ are given in Table 8, whereas the weight functions are shown in Table 9.

Combining the exergy analysis and $LCA$, the balance of the environmental impact for the $k$th component, including all input (or fuel) and output streams (product) of the jth, is given as [29]:

$$\sum \dot{B}_{j,k,in} + \dot{Y}_k = \sum \dot{B}_{j,k,out} \tag{37}$$

where $\dot{B}_j$ and $\dot{Y}_j$ are the $^{\text{jth}}$ stream-related and component-related environmental impacts:

$$\dot{B}_j = b_j \dot{E}x_j \tag{38}$$

**Table 6**
Exergoeconomic cost balances and auxiliary equation of the GDHS.

| Components | Cost balance | Auxiliary equation |
|---|---|---|
| T-line | $\dot{C}_1 + \dot{C}_{W,P1} + \dot{Z}_{T-line} = \dot{C}_2$ | $c_1 = 0$ |
| | | $c_{W,P1} = 0.5 \frac{\$}{MJ}$ |
| C | $\dot{C}_2 + \dot{C}_7 + \dot{Z}_C = \dot{C}_3 + \dot{C}_4$ | $c_2 = c_3$ |
| H-line | $\dot{C}_4 + \dot{C}_6 + \dot{C}_{W,P2} + \dot{Z}_{H-line} = \dot{C}_5 + \dot{C}_7$ | $c_6 = c_7$ |
| | | $c_{W,P2} = 0.5 \frac{\$}{MJ}$ |
| RS | $\dot{C}_5 + \dot{C}_{11} + \dot{C}_{W,P3} + \dot{Z}_{TES} = \dot{C}_6 + \dot{C}_8$ | $c_6 = c_7$ |
| | $\dot{C}_8 + \dot{C}_{W,Comp} + \dot{Z}_{Comp} = \dot{C}_9$ | |
| | $\dot{C}_9 + \dot{C}_{13} + \dot{Z}_{Con} = \dot{C}_{10} + \dot{C}_{12}$ | $c_{W,P3} = 0.5 \frac{\$}{MJ}$ |
| | $\dot{C}_{10} + \dot{Z}_V = \dot{C}_{11}$ | $c_{W,Comp} = 0.5 \frac{\$}{MJ}$ |
| HC | $\dot{C}_{12} + \dot{C}_{W,P4} + \dot{Z}_{PR} = \dot{C}_{13} + \dot{C}_{Q,PR}$ | $c_9 = c_{10}$ |
| | | $c_{W,P4} = 0.5 \frac{\$}{MJ}$ |
| | | $c_{Q,PR} = 0.0511 \frac{\$}{MJ}$ |
| ***Overall system*** | $\dot{C}_1 + \sum \dot{C}_W + \sum \dot{Z} = \dot{C}_3 + \dot{C}_Q$ | $c_W = 0.5 \frac{\$}{MJ}$ |
| | | $c_Q = 0.0511 \frac{\$}{MJ}$ |

**Table 7**
Cost functions of the components of GDHS.

| Components | Cost function | Reference |
|---|---|---|
| Pipe | $C_{pipe} = 5.231 \bullet 10^{-7}(d_{pipe})^3 - 3.06 \bullet 10^{-3}(d_{pipe})^2 + 1.940(d_{pipe}) - 6.106n_{pipe} - 209.567$ | – |
| HEx | $C_{Hex} = 12000\left(\frac{A_{HEx}}{100}\right)^{0.6}$ | [31] |
| TES (Eva) | $C_{TES} = 7.489 \bullet 10^{-7}(n_{pipe})^4 - 4.915 \bullet 10^{-4}(n_{pipe})^3 + 0.106(n_{pipe})^2 - 6.106n_{pipe} + 741.040$ | [22] |
| Con | $C_{Con} = -58.82(A_{Con})^2 - 487.34A_{condenser} + 112.11$ | – |
| Comp | $C_{Comp} = -92.4(\dot{W}_{Comp})^2 + 453.19\dot{W}_{compressor} + 28.01 \quad \text{for } \dot{W}_{compressor} \leq 1.5\ \text{kW}$ | – |
| P | $C_P = 2100\left(\frac{\dot{W}_P}{10}\right)^{0.26}\left(\frac{1-\eta}{\eta}\right)^{0.5}$ | [32] |
| PR | $C_{PR} = 5.231 \bullet 10^{-7}(d_{pipe})^3 - 3.06 \bullet 10^{-3}(d_{pipe})^2 + 1.940(d_{pipe}) - 6.106n_{pipe} - 209.567$ | – |

$$\dot{Y}_k = \dot{Y}_k^{CO} + \dot{Y}_k^{OM} + \dot{Y}_k^{D} \tag{39}$$

Here, $b_j$ denotes the specific environmental impact. $\dot{Y}_k^{CO}$, $\dot{Y}_k^{OM}$, and $\dot{Y}_k^{D}$ are environmental impacts of the life cycle phases including construction, operation and maintenance, and disposal, respectively. According to this, the average specific environmental impacts of the product ($b_{P,k}$) and fuel ($b_{F,k}$) and environmental impacts of exergy destruction for the $k$th component are given by:

$$\begin{aligned} b_{P,k} &= \frac{\dot{B}_{P,k}}{\dot{E}x_{P,k}} \\ b_{F,k} &= \frac{\dot{B}_{F,k}}{\dot{E}x_{F,k}} \\ \dot{B}_{d,k} &= b_{F,k}\dot{E}x_{d,k} \end{aligned} \tag{40}$$

As in the exergoeconomic evaluation, relative specific environmental impacts ($r_{b,k}$) and exergoenvironmental factors ($f_{b,k}$) are the essential parameters of the exergy-based assessment of the systems [29]. These parameters are given by:

$$r_{b,k} = \frac{b_{P,k} - b_{F,k}}{b_{F,k}} \tag{41}$$

$$f_{b,k} = \frac{\dot{Y}_k}{\dot{Y}_k + \dot{B}_{d,k}} \tag{42}$$

The other important parameter is the sustainability index ($SI$), which relates exergy to environmental impact since it enables us to see the reducing the use of resources and prolonging the resources' life. In terms of the exergy efficiency, SI is given as [63]:

$$SI = \frac{1}{1-\varepsilon} \tag{43}$$

Environmental impact balances and auxiliary equations of the GDHS are given in Table 10.

### 2.5. Efficiency analysis technique with output satisficing (EATWOS)

For the determination of the most efficient design of energy systems, Multi-Criteria Decision Making (MCDM) analysis is a powerful tool since it enables to evaluate the multiple criteria on an output basis [64]. EATWOS works to obtain the maximum outputs considering the minimum values of the inlet parameters. In this regard, EATWOS can be successfully applied with satisfactory results for energy problems [65,66]. In terms of the input weights ($w_k$), output weights ($v_j$), input distances ($ip_{ik}$), and output distances ($op_{ik}$), the efficiency value is given by Ref. [67]:

$$E_i = \frac{\sum_{j=1}^{J} v_j \bullet op_{ij}}{\sum_{k=1}^{K} w_k \bullet ip_{ik}} \tag{43b}$$

where,

$$ip_{ik} = 1 + \frac{x_{ik}}{\sqrt{\sum_{i=1}^{K} x_{ik}^2}} - \min_i\{s_k\} \tag{44}$$

**Table 8**
Component-related environmental impacts in *LCA* [60–62].

| Component | | Compounds | Composition | Eco'99 indicator (mPts/kg) | Material (mPts/kg) | Disposal (mPts/kg) | Total (mPts/kg) |
|---|---|---|---|---|---|---|---|
| **T-line** | **Pipe** | Steel low alloy | 1.5% | 110.00 | 86.36 | −5.90 | 80.46 |
| | | Steel | 98.5% | 86.00 | | | |
| | | Insulation (PUR) | 100.0% | 420.00 | 420.00 | 2.80 | 422.80 |
| | | Cover (PE) | 100.0% | 330.00 | 330.00 | −1.10 | 328.90 |
| | **$P_1$** | Steel | 35.0% | 86.00 | 186.10 | −5.90 | 146.30 |
| | | Cast iron | 65.0% | 240.00 | | −70.00 | |
| **C** | **HEx** | Steel | 26.0% | 86.00 | 695.76 | −5.90 | 689.86 |
| | | Steel high alloy | 74.0% | 910.00 | | | |
| **H-line** | **Pipe** | Steel low alloy | 1.5% | 110.00 | 86.36 | −5.90 | 80.46 |
| | | Steel | 98.5% | 86.00 | | | |
| | | Insulation (PUR) | 100.0% | 420.00 | 420.00 | 2.80 | 422.80 |
| | | Cover (PE) | 100.0% | 330.00 | 330.00 | −1.10 | 328.90 |
| | **$P_2$** | Steel | 35.0% | 86.00 | 186.10 | −5.90 | 138.54 |
| | | Cast iron | 65.0% | 240.00 | | −70.00 | |
| **RS** | **Eva (TES)** | Paraffin | 100.0% | 99.00 | – | – | 99.00 |
| | | Refrigerant (R600a) | 100.0% | 23000.00 | – | – | 23000.00 |
| | | Refrigerant (R290) | 100.0% | 23000.00 | – | – | 23000.00 |
| | | Refrigerant (1234ze) | 100.0% | 22970.00 | – | – | 22970.00 |
| | | Steel low alloy | 1.5% | 110.00 | 86.36 | −5.90 | 80.46 |
| | | Steel | 98.5% | 86.00 | | | |
| | | Insulation (Rock wool) | 100.0% | 61.00 | 61.00 | 5.10 | 66.10 |
| | | Cover (aluminium) | 100.0% | 780.00 | 780.00 | −23.00 | 757.00 |
| | **Comp** | Steel | 33.0% | 86.00 | 130.68 | −5.90 | 110.68 |
| | | Steel low alloy | 45.0% | 110.00 | | −5.90 | |
| | | Cast iron | 22.0% | 240.00 | | −70.00 | |
| | **Con** | Steel | 100.0% | 86.00 | 86.00 | −5.90 | 80.10 |
| | **P3** | Steel | 35.0% | 86.00 | 186.10 | −5.90 | 138.54 |
| | | Cast iron | 65.0% | 240.00 | | −70.00 | |
| **HC** | **PR** | Stell | 100.0% | 86.00 | 86.00 | −5.90 | 80.10 |
| | **P4** | Steel | 35.0% | 86.00 | 186.10 | −5.90 | 138.54 |
| | | Cast iron | 65.0% | 240.00 | | −70.00 | |

**Table 9**
Weight function of the components.

| Component | Weight function (kg) |
|---|---|
| **Pipe** | $w_{pipe} = [\pi L(r^2_{pipe,outer} - r^2_{pipe,inner})]8000$ [37] |
| **P** | $w_P = 6.1(\dot{W}_P^{0.95})$ [31] |
| **HEx** | $w_{Hex} = 850 + 3.8(N_{plate})$ [37] |
| **Eva (TES)** | $w_{TES} = \pi L[8000((r^2_{pipe,outer} - r^2_{pipe,inner})(n_{cooling} + n_{heating})) + ((r^2_{shell,outer} - r^2_{shell,inner})) + 150(r^2_{insulation,outer} - r^2_{insulation,inner}) + 2700(r^2_{cover,outer} - r^2_{cover,inner})]$ |
| **Comp** | $w_{Comp} = \frac{100 \bullet P \bullet d \bullet FS}{2\sigma}$ with $d$: equivalent diameter for m with 15 m/s; $FS$: safety factor with 2; $\sigma$: rupturing stress of 16 [32] |
| **Con** | $w_{Con} = 0.073(\dot{Q}_{Con})^{0.99}$ [31] |
| **PR** | $w_{Hex} = 33.7(L_{PR})$ [37] |

**Table 10**
Environmental impact balances of the GDHS.

| Components | Balance equation | Auxiliary equation |
|---|---|---|
| T-line | $\dot{B}_1 + \dot{B}_{W,P1} + \dot{Y}_{T-line} = \dot{B}_2$ | $b_1 = 0$ |
| | | $b_{W,P1} = 7.5\ \frac{mPts}{MJ}$ [62] |
| C | $\dot{B}_2 + \dot{B}_7 + Y_C = \dot{B}_3 + \dot{B}_4$ | $b_2 = b_3$ |
| H-line | $\dot{B}_4 + \dot{B}_6 + \dot{B}_{W,P2} + \dot{Y}_{H-line} = \dot{B}_5 + \dot{B}_7$ | $b_6 = b_7$ |
| | | $b_{W,P2} = 7.5\ \frac{mPts}{MJ}$ |
| RS | $\dot{B}_5 + \dot{B}_{11} + \dot{B}_{W,P3} + \dot{Y}_{TES} = \dot{B}_6 + \dot{B}_8$<br>$\dot{B}_8 + \dot{B}_{W,Comp} + \dot{Y}_{Comp} = \dot{B}_9$<br>$\dot{B}_9 + \dot{B}_{13} + \dot{Y}_{Con} = \dot{B}_{10} + \dot{B}_{12}$<br>$\dot{B}_{10} + \dot{Y}_V = \dot{B}_{11}$ | $b_6 = b_7$ |
| | | $b_{W,P3} = 7.5\ \frac{mPts}{MJ}$ |
| | | $b_{W,Comp} = 7.5\ \frac{mPts}{MJ}$ |
| HC | $\dot{B}_{12} + \dot{B}_{W,P4} + \dot{Y}_{PR} = \dot{B}_{13} + \dot{B}_{Q,PR}$ | $b_9 = b_{10}$ |
| | | $b_{W,P4} = 7.5\ \frac{mPts}{MJ}$ |
| | | $b_{Q,PR} = 5.4\ \frac{mPts}{MJ}$ [62] |
| ***Overall system*** | $\dot{B}_1 + \sum \dot{B}_W + \sum \dot{Y} = \dot{B}_3 + \dot{B}_Q$ | $b_W = 7.5\ \frac{mPts}{MJ}$ |
| | | $b_Q = 5.4\ \frac{mPts}{MJ}$ |

$$op_{ik} = 1 + \frac{y_{ij}}{\sqrt{\sum_{i=1}^{I} y_{ik}^2}} - \max_i \{r_j\} \tag{45}$$

where $s_{ik}$, $r_{ij}$, $s_k^*$, and $r_j^*$ are normalized input, normalized output, maximum normalized input, and maximum normalized output values, respectively. The inlet and outlet parameters are given in Table 11.

## 3. Results and discussion

The designed GDHS system was evaluated regarding exergy, environment, and economic factors to determine the optimum solution. One hundred eleven (111) cases were formed considering the working fluids and conditions in this aim. The cases were formed in the range of available limits depending on the different temperature scales. The temperature scales were tried to be kept the same or closer for all the fluid types. In this respect, the inlet temperature of T-line ($T_1$), the inlet and outlet temperature of the refrigerant ($T_{10}$ and $T_{11}$), inlet and outlet temperature of PR ($T_{12}$ and $T_{13}$) were operated as the main deterministic parameter. In HEx, a temperature

**Table 11**
The inlet and outlet parameters.

| Inlet parameter | Modified inlet parameters | Outlet parameters | Modified inlet parameters |
|---|---|---|---|
| $T_1$ | $T_1$ | $f$ | $f$ |
| $T_3$ | $1/(T_1 - T_3)$ | $f_b$ | $f_b$ |
| $T_5$ | $1/(T_5 - T_8)$ | $r$ | $1/r$ |
| $T_6$ | $1/T_6$ | $r_b$ | $1/r_b$ |
| $T_{12}$ | $T_{12}$ | $SI$ | $SI$ |
| $T_{13}$ | $1/(T_{12} - T_{13})$ | | |
| $T_8$ | $1/(T_8 - T_{11})$ | | |
| $T_{11}$ | | | |

**Table 12**
The formed cases for R600a.

| Cases | $\Delta T_{min}$ | $T_m$ | $T_1$ | $T_2$ | $T_3$ | $T_4$ | $T_5$ | $T_6$ | $T_7$ | $T_8$ | $T_9$ | $T_{10}$ | $T_{11}$ | $T_{12}$ | $T_{13}$ | $P_8$=$P_{11}$ | $P_9$=$P_{10}$ |
|---|---|---|---|---|---|---|---|---|---|---|---|---|---|---|---|---|---|
| 1 | 15.76 | 60 | 100 | 99.89 | 72.00 | 94.89 | 94.80 | 67 | 66.94 | 40 | 70.76 | 70 | 33 | 55 | 40 | 440.01 | 1087.50 |
| 2 | 18.81 | 60 | 100 | 99.89 | 71.73 | 94.89 | 94.80 | 66 | 65.94 | 45 | 73.81 | 70 | 35 | 55 | 40 | 464.77 | 1087.50 |
| 3 | 15.85 | 60 | 100 | 99.89 | 70.62 | 94.89 | 94.80 | 65 | 64.94 | 40 | 60.85 | 50 | 25 | 45 | 30 | 350.67 | 684.90 |
| 4 | 15.01 | 60 | 100 | 99.89 | 70.51 | 94.89 | 94.80 | 65 | 64.94 | 40 | 60.01 | 50 | 26 | 45 | 30 | 361.02 | 684.90 |
| 5 | 15.79 | 60 | 100 | 99.89 | 70.61 | 94.89 | 94.80 | 65 | 64.94 | 40 | 60.79 | 55 | 30 | 45 | 30 | 404.72 | 772.99 |
| 6 | 15.00 | 60 | 100 | 99.89 | 71.11 | 94.89 | 94.80 | 65 | 64.94 | 45 | 70.44 | 60 | 29 | 55 | 45 | 393.45 | 869.16 |
| 7 | 15.00 | 70 | 110 | 109.87 | 80.93 | 104.87 | 104.78 | 75 | 74.93 | 55 | 75.26 | 55 | 30 | 60 | 40 | 404.72 | 772.99 |
| 8 | 19.20 | 70 | 110 | 109.87 | 81.46 | 104.87 | 104.78 | 75 | 74.93 | 55 | 79.20 | 60 | 30 | 60 | 40 | 404.72 | 869.16 |
| 9 | 15.71 | 55 | 95 | 94.89 | 66.51 | 89.89 | 89.81 | 60 | 59.95 | 40 | 65.71 | 61 | 30 | 50 | 40 | 404.72 | 889.40 |
| 10 | 15.79 | 55 | 95 | 94.89 | 65.84 | 89.89 | 89.81 | 60 | 59.95 | 40 | 60.79 | 55 | 30 | 45 | 35 | 404.72 | 772.99 |
| 11 | 10.25 | 55 | 100 | 99.89 | 71.05 | 94.89 | 94.80 | 66 | 65.94 | 43 | 65.25 | 60 | 33 | 55 | 40 | 440.01 | 869.16 |
| 12 | 11.39 | 60 | 100 | 99.89 | 70.02 | 94.89 | 94.80 | 65 | 64.95 | 50 | 66.39 | 60 | 40 | 55 | 40 | 531.21 | 869.16 |
| 13 | 10.61 | 60 | 100 | 99.89 | 70.55 | 94.89 | 94.80 | 65 | 64.94 | 45 | 65.61 | 60 | 35 | 55 | 40 | 464.77 | 869.16 |
| 14 | 10.59 | 55 | 100 | 99.89 | 70.83 | 94.89 | 94.80 | 65 | 64.94 | 45 | 65.59 | 55 | 30 | 55 | 40 | 404.80 | 772.99 |
| 15 | 12.56 | 60 | 100 | 99.89 | 70.19 | 94.89 | 94.80 | 65 | 64.95 | 40 | 57.56 | 47 | 26 | 45 | 30 | 361.02 | 635.74 |
| 16 | 17.00 | 60 | 100 | 99.89 | 70.04 | 94.89 | 94.80 | 65 | 64.95 | 50 | 66.49 | 47 | 27 | 45 | 30 | 371.60 | 635.74 |
| 17 | 10.00 | 60 | 100 | 99.89 | 70.59 | 94.89 | 94.80 | 65 | 64.94 | 45 | 65.59 | 55 | 30 | 55 | 45 | 404.72 | 772.99 |
| 18 | 10.00 | 60 | 100 | 99.89 | 70.70 | 94.89 | 94.80 | 65 | 64.94 | 45 | 66.41 | 55 | 29 | 55 | 45 | 393.45 | 772.99 |
| 19 | 10.00 | 70 | 110 | 109.87 | 80.41 | 104.87 | 104.78 | 75 | 74.94 | 55 | 71.30 | 50 | 30 | 60 | 40 | 404.72 | 684.90 |
| 20 | 11.20 | 70 | 110 | 109.87 | 80.40 | 104.87 | 104.78 | 75 | 74.94 | 55 | 71.20 | 60 | 40 | 60 | 40 | 531.21 | 869.16 |
| 21 | 10.41 | 70 | 110 | 109.87 | 80.29 | 104.87 | 104.78 | 75 | 74.94 | 55 | 70.41 | 60 | 41 | 60 | 40 | 545.30 | 869.16 |
| 22 | 10.41 | 70 | 110 | 109.87 | 80.30 | 104.87 | 104.78 | 75 | 74.94 | 55 | 70.41 | 54 | 35 | 60 | 40 | 464.77 | 754.74 |
| 23 | 10.79 | 55 | 95 | 94.89 | 65.84 | 89.89 | 89.81 | 60 | 59.95 | 40 | 60.79 | 55 | 30 | 50 | 40 | 404.72 | 772.99 |
| 24 | 10.05 | 55 | 95 | 94.89 | 65.08 | 89.89 | 89.81 | 60 | 59.95 | 40 | 55.05 | 48 | 30 | 45 | 35 | 404.72 | 651.82 |
| 25 | 10.00 | 55 | 100 | 99.89 | 70.34 | 94.89 | 94.80 | 65 | 64.94 | 40 | 56.94 | 40 | 20 | 45 | 30 | 302.22 | 531.21 |
| 26 | 6.39 | 60 | 100 | 99.89 | 70.02 | 94.89 | 94.80 | 65 | 64.95 | 50 | 66.39 | 60 | 40 | 60 | 50 | 531.21 | 869.16 |
| 27 | 5.61 | 60 | 100 | 99.89 | 70.55 | 94.89 | 94.80 | 65 | 64.94 | 45 | 65.61 | 60 | 35 | 60 | 50 | 464.77 | 869.16 |
| 28 | 5.00 | 60 | 100 | 99.89 | 70.05 | 94.89 | 94.80 | 65 | 64.95 | 45 | 61.55 | 50 | 30 | 55 | 45 | 404.72 | 684.90 |
| 29 | 5.00 | 70 | 110 | 109.87 | 80.40 | 104.87 | 104.78 | 75 | 74.94 | 55 | 71.20 | 60 | 40 | 65 | 55 | 531.21 | 869.16 |
| 30 | 5.00 | 70 | 110 | 109.87 | 80.29 | 104.87 | 104.78 | 75 | 74.94 | 55 | 70.41 | 60 | 41 | 65 | 55 | 545.30 | 869.16 |
| 31 | 5.41 | 70 | 110 | 109.87 | 80.30 | 104.87 | 104.78 | 75 | 74.94 | 55 | 70.41 | 54 | 35 | 65 | 45 | 464.77 | 754.74 |
| 32 | 5.05 | 55 | 95 | 94.89 | 65.08 | 89.89 | 89.81 | 60 | 59.95 | 40 | 55.05 | 48 | 30 | 50 | 40 | 404.72 | 651.82 |
| 33 | 5.05 | 55 | 95 | 94.89 | 65.08 | 89.89 | 89.81 | 60 | 59.95 | 40 | 55.05 | 48 | 30 | 50 | 35 | 404.72 | 651.82 |
| 34 | 5.00 | 70 | 110 | 109.87 | 80.40 | 104.87 | 104.78 | 75 | 74.94 | 55 | 71.21 | 55 | 35 | 65 | 50 | 464.77 | 772.99 |
| 35 | 6.55 | 60 | 100 | 99.89 | 70.05 | 94.89 | 94.80 | 65 | 64.95 | 45 | 61.55 | 50 | 30 | 55 | 40 | 404.72 | 684.90 |
| 36 | 6.55 | 60 | 100 | 99.89 | 70.05 | 94.89 | 94.80 | 65 | 64.95 | 45 | 61.55 | 50 | 30 | 55 | 35 | 404.72 | 684.90 |
| 37 | 6.21 | 70 | 110 | 109.87 | 80.40 | 104.87 | 104.78 | 75 | 74.94 | 55 | 71.21 | 55 | 35 | 65 | 45 | 464.77 | 772.99 |

**Table 13**
The formed cases for R290.

| Cases | $\Delta T_{min}$ | $T_m$ | $T_1$ | $T_2$ | $T_3$ | $T_4$ | $T_5$ | $T_6$ | $T_7$ | $T_8$ | $T_9$ | $T_{10}$ | $T_{11}$ | $T_{12}$ | $T_{13}$ | $P_8$=$P_{11}$ | $P_9$=$P_{10}$ |
|---|---|---|---|---|---|---|---|---|---|---|---|---|---|---|---|---|---|
| 38 | 24.80 | 60 | 100 | 99.89 | 72.41 | 94.89 | 94.80 | 67 | 66.94 | 40 | 79.94 | 70 | 33 | 55 | 40 | 1160.80 | 2586.80 |
| 39 | 24.80 | 60 | 100 | 99.89 | 72.11 | 94.89 | 94.80 | 66 | 65.94 | 45 | 82.34 | 70 | 35 | 55 | 40 | 1217.90 | 2586.80 |
| 40 | 20.00 | 60 | 100 | 99.89 | 70.79 | 94.89 | 94.80 | 65 | 64.94 | 40 | 66.38 | 50 | 25 | 45 | 30 | 952.07 | 1716.30 |
| 41 | 20.00 | 60 | 100 | 99.89 | 70.67 | 94.89 | 94.80 | 65 | 64.94 | 40 | 65.30 | 50 | 26 | 45 | 30 | 976.53 | 1713.30 |
| 42 | 21.58 | 60 | 100 | 99.89 | 71.17 | 94.89 | 94.80 | 65 | 64.94 | 40 | 66.58 | 55 | 30 | 45 | 30 | 1079.00 | 1907.20 |
| 43 | 15.00 | 60 | 100 | 99.89 | 71.51 | 94.89 | 94.80 | 65 | 64.94 | 45 | 77.37 | 60 | 29 | 55 | 45 | 1052.70 | 2116.80 |
| 44 | 15.00 | 70 | 110 | 109.87 | 81.13 | 104.87 | 104.78 | 75 | 74.93 | 55 | 80.56 | 55 | 30 | 60 | 40 | 1079.00 | 1907.20 |
| 45 | 20.00 | 70 | 110 | 109.87 | 81.73 | 104.87 | 104.78 | 75 | 74.93 | 55 | 85.64 | 60 | 30 | 60 | 40 | 1079.00 | 2116.80 |
| 46 | 21.00 | 55 | 95 | 94.89 | 66.77 | 89.89 | 89.81 | 60 | 59.95 | 40 | 72.97 | 61 | 30 | 50 | 40 | 1079.00 | 2160.60 |
| 47 | 20.00 | 55 | 95 | 94.89 | 66.02 | 89.89 | 89.81 | 60 | 59.95 | 40 | 66.58 | 55 | 30 | 45 | 35 | 1079.00 | 1907.20 |
| 48 | 16.71 | 55 | 100 | 99.89 | 71.28 | 94.89 | 94.80 | 66 | 65.94 | 43 | 71.71 | 60 | 33 | 55 | 40 | 1160.80 | 2116.80 |
| 49 | 16.29 | 60 | 100 | 99.89 | 70.30 | 94.89 | 94.80 | 65 | 64.94 | 50 | 71.29 | 60 | 40 | 55 | 40 | 1369.40 | 2116.80 |
| 50 | 16.59 | 60 | 100 | 99.89 | 70.80 | 94.89 | 94.80 | 65 | 64.94 | 45 | 71.59 | 60 | 35 | 55 | 40 | 1217.90 | 2116.80 |
| 51 | 15.00 | 55 | 100 | 99.89 | 71.02 | 94.89 | 94.80 | 65 | 64.94 | 45 | 71.19 | 55 | 30 | 55 | 40 | 1079.00 | 1907.20 |
| 52 | 17.00 | 60 | 100 | 99.89 | 70.32 | 94.89 | 94.80 | 65 | 64.94 | 40 | 62.16 | 47 | 26 | 45 | 30 | 976.53 | 1604.20 |
| 53 | 17.00 | 60 | 100 | 99.89 | 70.18 | 94.89 | 94.80 | 65 | 64.95 | 50 | 70.68 | 47 | 27 | 45 | 30 | 1001.40 | 1604.20 |
| 54 | 10.00 | 60 | 100 | 99.89 | 70.78 | 94.89 | 94.80 | 65 | 64.94 | 45 | 71.19 | 55 | 30 | 55 | 45 | 1079.00 | 1907.20 |
| 55 | 10.00 | 60 | 100 | 99.89 | 70.89 | 94.89 | 94.80 | 65 | 64.94 | 45 | 72.17 | 55 | 29 | 55 | 45 | 1052.70 | 1907.20 |
| 56 | 10.00 | 70 | 110 | 109.87 | 80.56 | 104.87 | 104.78 | 75 | 74.94 | 55 | 75.50 | 50 | 30 | 60 | 40 | 1079.00 | 1713.30 |
| 57 | 15.91 | 70 | 110 | 109.87 | 80.58 | 104.87 | 104.78 | 75 | 74.94 | 55 | 75.91 | 60 | 40 | 60 | 40 | 1369.40 | 2116.80 |
| 58 | 14.93 | 70 | 110 | 109.87 | 80.46 | 104.87 | 104.78 | 75 | 74.94 | 55 | 74.93 | 60 | 41 | 60 | 40 | 1401.30 | 2116.80 |
| 59 | 14.00 | 70 | 110 | 109.87 | 80.44 | 104.87 | 104.78 | 75 | 74.94 | 55 | 74.61 | 54 | 35 | 60 | 40 | 1217.90 | 1867.20 |
| 60 | 15.00 | 55 | 95 | 94.89 | 66.02 | 89.89 | 89.81 | 60 | 59.95 | 40 | 66.58 | 55 | 30 | 50 | 40 | 1079.00 | 1907.20 |
| 61 | 13.00 | 55 | 95 | 94.89 | 65.20 | 89.89 | 89.81 | 60 | 59.95 | 40 | 59.15 | 48 | 30 | 45 | 35 | 1079.00 | 1640.00 |
| 62 | 10.00 | 55 | 100 | 99.89 | 70.45 | 94.89 | 94.80 | 65 | 64.94 | 40 | 61.05 | 40 | 20 | 45 | 30 | 836.46 | 1369.40 |
| 63 | 10.00 | 60 | 100 | 99.89 | 70.19 | 94.89 | 94.80 | 65 | 64.95 | 50 | 71.29 | 60 | 40 | 60 | 50 | 1369.40 | 2116.80 |
| 64 | 10.00 | 60 | 100 | 99.89 | 70.80 | 94.89 | 94.80 | 65 | 64.94 | 45 | 71.59 | 60 | 35 | 60 | 50 | 1217.90 | 2116.80 |
| 65 | 5.00 | 60 | 100 | 99.89 | 70.19 | 94.89 | 94.80 | 65 | 64.95 | 45 | 65.97 | 50 | 30 | 55 | 45 | 1079.00 | 1713.30 |
| 66 | 5.00 | 70 | 110 | 109.87 | 80.58 | 104.87 | 104.78 | 75 | 74.94 | 55 | 75.91 | 60 | 40 | 65 | 55 | 1369.40 | 2116.80 |
| 67 | 5.00 | 70 | 110 | 109.87 | 80.46 | 104.87 | 104.78 | 75 | 74.94 | 55 | 74.93 | 60 | 41 | 65 | 55 | 1401.30 | 2116.80 |
| 68 | 9.00 | 70 | 110 | 109.87 | 80.45 | 104.87 | 104.78 | 75 | 74.94 | 55 | 74.61 | 54 | 35 | 65 | 45 | 1217.90 | 1867.20 |
| 69 | 8.00 | 55 | 95 | 94.89 | 65.20 | 89.89 | 89.81 | 60 | 59.95 | 40 | 59.15 | 48 | 30 | 50 | 40 | 1079.00 | 1640.00 |
| 70 | 9.19 | 55 | 95 | 94.89 | 65.20 | 89.89 | 89.81 | 60 | 59.95 | 40 | 59.19 | 48 | 30 | 50 | 35 | 1079.00 | 1640.00 |
| 71 | 5.00 | 70 | 110 | 109.87 | 80.56 | 104.87 | 104.78 | 75 | 74.94 | 55 | 75.64 | 55 | 35 | 65 | 50 | 1217.90 | 1907.20 |
| 72 | 10.00 | 60 | 100 | 99.89 | 70.19 | 94.89 | 94.80 | 65 | 64.95 | 45 | 66.97 | 50 | 30 | 55 | 40 | 1079.00 | 1713.30 |
| 73 | 10.97 | 60 | 100 | 99.89 | 70.19 | 94.89 | 94.80 | 65 | 64.95 | 45 | 65.97 | 50 | 30 | 55 | 35 | 1079.00 | 1713.30 |
| 74 | 10.00 | 70 | 110 | 109.87 | 80.56 | 104.87 | 104.78 | 75 | 74.94 | 55 | 75.64 | 55 | 35 | 65 | 45 | 1217.90 | 1907.20 |

**Table 14**
The formed cases for R1234ze.

| Cases | $\Delta T_{min}$ | $T_m$ | $T_1$ | $T_2$ | $T_3$ | $T_4$ | $T_5$ | $T_6$ | $T_7$ | $T_8$ | $T_9$ | $T_{10}$ | $T_{11}$ | $T_{12}$ | $T_{13}$ | $P_8$=$P_{11}$ | $P_9$=$P_{10}$ |
|---|---|---|---|---|---|---|---|---|---|---|---|---|---|---|---|---|---|
| 75 | 19.71 | 60 | 100 | 99.89 | 72.20 | 94.89 | 94.80 | 67 | 66.94 | 40 | 74.71 | 70 | 33 | 55 | 40 | 630.75 | 1611.10 |
| 76 | 22.50 | 60 | 100 | 99.89 | 71.91 | 94.89 | 94.80 | 66 | 65.94 | 45 | 77.50 | 70 | 35 | 55 | 40 | 667.56 | 1611.10 |
| 77 | 17.79 | 55 | 100 | 99.89 | 70.93 | 94.89 | 94.80 | 65 | 64.94 | 40 | 62.79 | 50 | 25 | 45 | 30 | 498.59 | 997.45 |
| 78 | 16.91 | 60 | 100 | 99.89 | 70.57 | 94.89 | 94.80 | 65 | 64.94 | 40 | 61.91 | 50 | 26 | 45 | 30 | 513.85 | 997.45 |
| 79 | 17.99 | 60 | 100 | 99.89 | 70.69 | 94.89 | 94.80 | 65 | 64.94 | 40 | 62.99 | 55 | 30 | 45 | 30 | 578.43 | 1130.70 |
| 80 | 15.00 | 60 | 100 | 99.89 | 71.36 | 94.89 | 94.80 | 65 | 64.94 | 45 | 73.16 | 60 | 29 | 55 | 45 | 561.75 | 1276.80 |
| 81 | 15.00 | 70 | 110 | 109.87 | 81.01 | 104.87 | 104.78 | 75 | 74.93 | 55 | 77.31 | 55 | 30 | 60 | 40 | 578.43 | 1130.70 |
| 82 | 20.00 | 70 | 110 | 109.87 | 81.57 | 104.87 | 104.78 | 75 | 74.93 | 55 | 81.75 | 60 | 30 | 60 | 40 | 578.43 | 1276.80 |
| 83 | 18.58 | 55 | 95 | 94.89 | 66.63 | 89.89 | 89.81 | 60 | 59.95 | 40 | 68.58 | 61 | 30 | 50 | 40 | 578.43 | 1307.70 |
| 84 | 17.99 | 55 | 95 | 94.89 | 65.91 | 89.89 | 89.81 | 60 | 59.95 | 40 | 62.99 | 55 | 30 | 45 | 35 | 578.43 | 1130.70 |
| 85 | 12.86 | 55 | 100 | 99.89 | 71.16 | 94.89 | 94.80 | 66 | 65.94 | 43 | 67.86 | 60 | 33 | 55 | 40 | 630.75 | 1276.80 |
| 86 | 13.41 | 60 | 100 | 99.89 | 70.09 | 94.89 | 94.80 | 65 | 64.95 | 50 | 68.41 | 60 | 40 | 55 | 40 | 630.75 | 1276.80 |
| 87 | 13.01 | 60 | 100 | 99.89 | 70.68 | 94.89 | 94.80 | 65 | 64.94 | 45 | 68.01 | 60 | 35 | 55 | 40 | 667.56 | 1276.80 |
| 88 | 10.59 | 55 | 100 | 99.89 | 70.91 | 94.89 | 94.80 | 65 | 64.94 | 45 | 65.59 | 55 | 30 | 55 | 40 | 578.43 | 1130.70 |
| 89 | 14.18 | 60 | 100 | 99.89 | 70.24 | 94.89 | 94.80 | 65 | 64.94 | 40 | 59.18 | 47 | 26 | 45 | 30 | 513.85 | 923.39 |
| 90 | 17.00 | 60 | 100 | 99.89 | 70.09 | 94.89 | 94.80 | 65 | 64.95 | 50 | 67.99 | 47 | 27 | 45 | 30 | 529.46 | 923.39 |
| 91 | 10.00 | 60 | 100 | 99.89 | 70.67 | 94.89 | 94.80 | 65 | 64.94 | 45 | 67.72 | 55 | 30 | 55 | 45 | 578.43 | 1130.70 |
| 92 | 10.00 | 60 | 100 | 99.89 | 70.78 | 94.89 | 94.80 | 65 | 64.94 | 45 | 68.60 | 55 | 29 | 55 | 45 | 561.75 | 1130.70 |
| 93 | 10.00 | 70 | 110 | 109.87 | 80.47 | 104.87 | 104.78 | 75 | 74.94 | 55 | 72.86 | 50 | 30 | 60 | 40 | 578.43 | 997.15 |
| 94 | 13.14 | 70 | 110 | 109.87 | 80.46 | 104.87 | 104.78 | 75 | 74.94 | 55 | 73.14 | 60 | 40 | 60 | 40 | 766.63 | 1276.80 |
| 95 | 12.28 | 70 | 110 | 109.87 | 80.36 | 104.87 | 104.78 | 75 | 74.94 | 55 | 72.28 | 60 | 41 | 60 | 40 | 787.70 | 1276.80 |
| 96 | 12.05 | 70 | 110 | 109.87 | 80.36 | 104.87 | 104.78 | 75 | 74.94 | 55 | 72.05 | 54 | 35 | 60 | 40 | 667.56 | 1103.00 |
| 97 | 12.99 | 55 | 95 | 94.89 | 65.91 | 89.89 | 89.81 | 60 | 59.95 | 40 | 62.99 | 55 | 30 | 50 | 40 | 578.43 | 1130.70 |
| 98 | 11.53 | 55 | 95 | 94.89 | 65.13 | 89.89 | 89.81 | 60 | 59.95 | 40 | 56.53 | 48 | 30 | 45 | 35 | 578.43 | 947.60 |
| 99 | 10.00 | 55 | 100 | 99.89 | 70.38 | 94.89 | 94.80 | 65 | 64.94 | 40 | 58.27 | 40 | 20 | 45 | 30 | 427.38 | 766.63 |
| 100 | 8.42 | 60 | 100 | 99.89 | 70.09 | 94.89 | 94.80 | 65 | 64.95 | 50 | 68.42 | 60 | 40 | 60 | 50 | 766.30 | 1276.80 |
| 101 | 8.01 | 60 | 100 | 99.89 | 70.68 | 94.89 | 94.80 | 65 | 64.94 | 45 | 68.01 | 60 | 35 | 60 | 50 | 667.56 | 1276.80 |
| 102 | 5.00 | 60 | 100 | 99.89 | 70.11 | 94.89 | 94.80 | 65 | 64.95 | 45 | 63.17 | 50 | 30 | 55 | 45 | 578.43 | 997.45 |
| 103 | 5.00 | 70 | 110 | 109.87 | 80.47 | 104.87 | 104.78 | 75 | 74.94 | 55 | 73.14 | 60 | 40 | 65 | 55 | 766.63 | 1276.80 |
| 104 | 5.00 | 70 | 110 | 109.87 | 80.36 | 104.87 | 104.78 | 75 | 74.94 | 55 | 72.28 | 60 | 41 | 65 | 55 | 787.70 | 1276.80 |
| 105 | 7.05 | 70 | 110 | 109.87 | 80.30 | 104.87 | 104.78 | 75 | 74.94 | 55 | 72.05 | 54 | 35 | 65 | 45 | 667.56 | 1103.00 |
| 106 | 6.53 | 55 | 95 | 94.89 | 65.13 | 89.89 | 89.81 | 60 | 59.95 | 40 | 56.53 | 48 | 30 | 50 | 40 | 578.43 | 947.60 |
| 107 | 5.05 | 55 | 95 | 94.89 | 65.13 | 89.89 | 89.81 | 60 | 59.95 | 40 | 55.05 | 48 | 30 | 50 | 35 | 578.43 | 947.60 |
| 108 | 5.00 | 70 | 110 | 109.87 | 80.47 | 104.87 | 104.78 | 75 | 74.94 | 55 | 72.94 | 55 | 35 | 65 | 50 | 667.56 | 1130.70 |
| 109 | 8.17 | 60 | 100 | 99.89 | 70.11 | 94.89 | 94.80 | 65 | 64.95 | 45 | 63.17 | 50 | 30 | 55 | 40 | 578.43 | 997.45 |
| 110 | 8.17 | 60 | 100 | 99.89 | 70.11 | 94.89 | 94.80 | 65 | 64.95 | 45 | 63.17 | 50 | 30 | 55 | 35 | 578.43 | 997.45 |
| 111 | 7.94 | 70 | 110 | 109.87 | 80.47 | 104.87 | 104.78 | 75 | 74.94 | 55 | 72.94 | 55 | 35 | 65 | 45 | 667.56 | 1130.70 |

difference of 5 °C was considered for an effective transfer since both fluids are in the liquid phase. For Eva and Con, the temperature differences between the inlet and outlet flows ($\Delta T_{min}$) were handled parametrically and tried to be kept minimally 5 °C, 10 °C and 15 °C to measure the size and operating effects. The pressure values were determined according to the saturated properties of points 10 and 11. The other values were calculated for the available limit values. The other values were calculated for the available limit values. The technical properties of formed cases are given in Table 12 for the dry-type refrigerant. The technical properties of formed cases for isentropic and wet-type refrigerants are shown in Tables 13 and 14, respectively.

According to the formed cases, the exergy analysis was performed using the energy and exergy balances given in Table 5. The obtained results of the exergy analysis are shown in Fig. 3.

According to Fig. 3, the exergy destruction in the T-line ranges between 1517.62–1601.97 kW, 1518.82–1605.25 kW, and 1518.12–1603.36 kW for R600a, R290, and R1234ze, respectively. The exergy destruction in the C ranges between 823.61 and 946.06 kW, 838.02–955.14 kW, and 830.30–950.27 kW for R600a, R290, and R1234ze, respectively. The exergy destruction in the H-line ranges between 9654.67–11,377.09 kW, 9364.66–11,159.08 kW and 9534.74–11,258.32 kW for R600a, R290, and R1234ze, respectively. The exergy destruction in the RS ranges between 8574.85–13,897.90 kW, 8877.43–14,735.09 kW and 8675.89–14,290.16 kW for R600a, R290, and R1234ze, respectively. The exergy destruction in the HC ranges between 127.99 and 909.83 kW, 121.91–820.69 kW, and 124.22–864.34 kW for R600a, R290, and R1234ze, respectively. For the overall system, the exergy destruction ranges between 23,002.03 and 27,924.19 kW, 23,108.97–28,298.56 kW and 23,002.21–28,093.18 kW for R600a, R290, and R1234ze, respectively. The minimum exergy destruction was determined for the case with R600a. These results show the main cause of exergy destruction is the HP-sourced ones due to higher power consumption. From the viewpoint of exergy analysis, the exergy efficiency values were determined and given in Fig. 4.

According to Fig. 4, the exergy efficiency in the T-line ranges between 90.00 and 92.60%, 89.99–92.59%, and 90.00–92.60% for R600a, R290, and R1234ze, respectively. The exergy efficiency in the C ranges between 89.08 and 91.95%, 88.90–91.86%, and 89.00–91.91% for R600a, R290, and R1234ze, respectively. The exergy efficiency in the H-line ranges between 57.86 and 69.96%, 58.04–70.34%, and 57.93–70.12% for R600a, R290, and R1234ze, respectively. The exergy efficiency in the RS ranges between 15.46 and 40.15%, 14.35–39.33%, and 15.30–39.87% for R600a, R290, and R1234ze, respectively. The exergy efficiency in the HC ranges between 76.30 and 97.57%, 76.94–97.68%, and 76.71–97.64% for R600a, R290, and R1234ze, respectively. For the overall system, the exergy efficiency ranges between 7.98 and 20.30%, 7.82–20.25%, and 7.96–20.29% for R600a, R290, and R1234ze, respectively. The maximum exergy efficiency of HP and the overall system was obtained for the case with R600a since the pump and compressor required power was relatively lower. However, the operating pressure range is limited due to the thermodynamic behaviour of R600a. From this point, the environmental benefits would be confined to a limited degree. So, the combined evaluations are necessary for sensitive decision-making for the optimal system design. The results of the exergoeconomic analysis are given in Figs. 5 and 6. The results of the exergoenvironmental analysis are shown in Figs. 7 and 8.

According to Fig. 5, the relative cost in the T-line ranges between 8.60 and 11.74%, 8.61–11.76%, and 8.60–11.75% for R600a, R290, and R1234ze, respectively. The relative cost in the C ranges between 10.92 and 42.96%, 10.98–14.23%, and 10.95–42.72% for R600a, R290, and R1234ze, respectively. The relative cost in the H-line ranges between 43.26 and 73.18%, 42.49–72.65%, and 42.93–72.98% for R600a, R290, and R1234ze, respectively. The relative cost in the RS ranges between 166.16 and 581.20%, 170.39–631.46%, and 167.43–585.93% for R600a, R290, and R1234ze, respectively. The relative cost in the HC ranges between 5.76 and 35.86%, 5.64–34.74%, and 5.69–35.15% for R600a, R290, and R1234ze, respectively. The overall system's relative cost ranges between 429.02 and 1260.76%, 427.95–1268.45%, and 428.15–1263.05% for R600a, R290, and R1234ze, respectively. These outputs clearly show that the RS system is the dominant component collimating economic action.

According to Fig. 6, the exergoeconomic factor in the T-line ranges between 0.001592 and 0.002094%, 0.001586–0.002089%, and 0.001589–0.002094% for R600a, R290, and R1234ze, respectively. The exergoeconomic factor in the C ranges between 0.004639 and

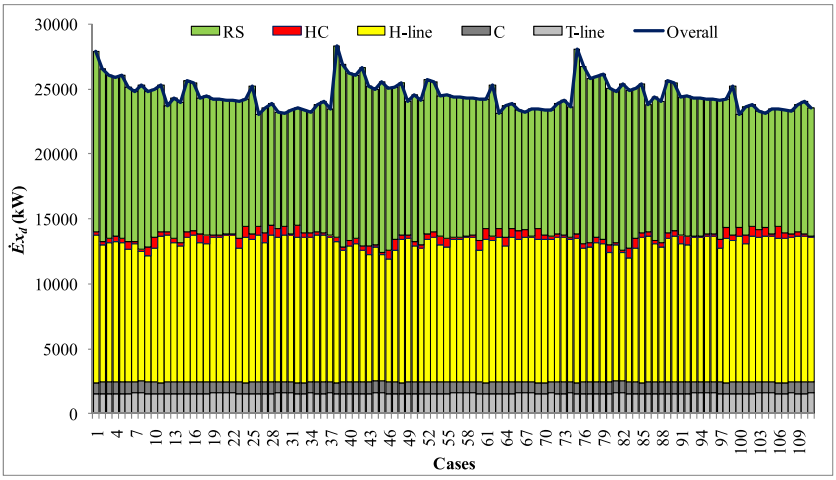


**Fig. 3.** Exergy destructions on the component basis for the formed cases.

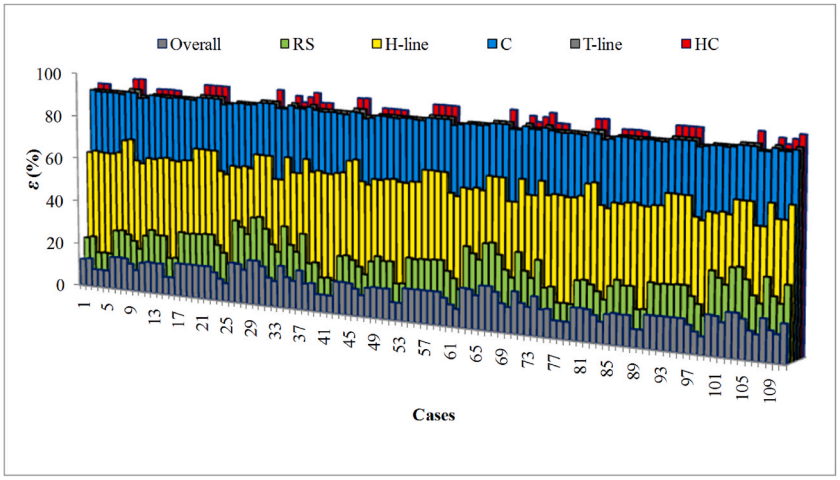


**Fig. 4.** Exergy efficiencies on the component basis for the formed cases.

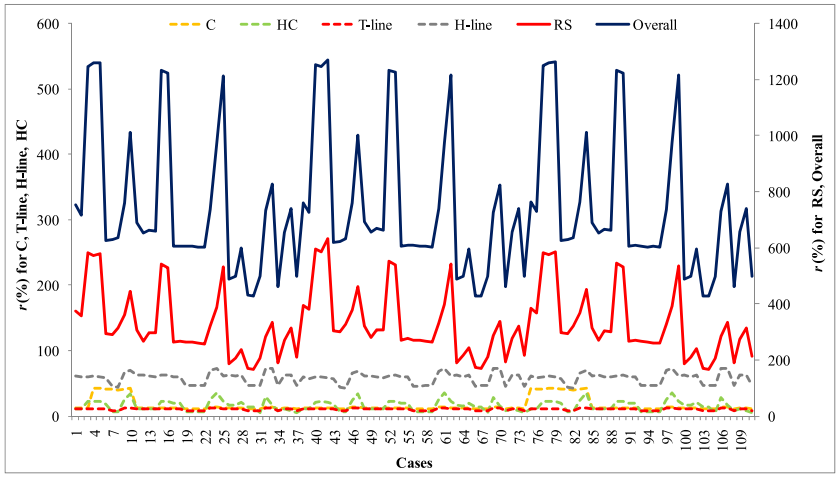


**Fig. 5.** Relative costs on the component basis for the formed cases.

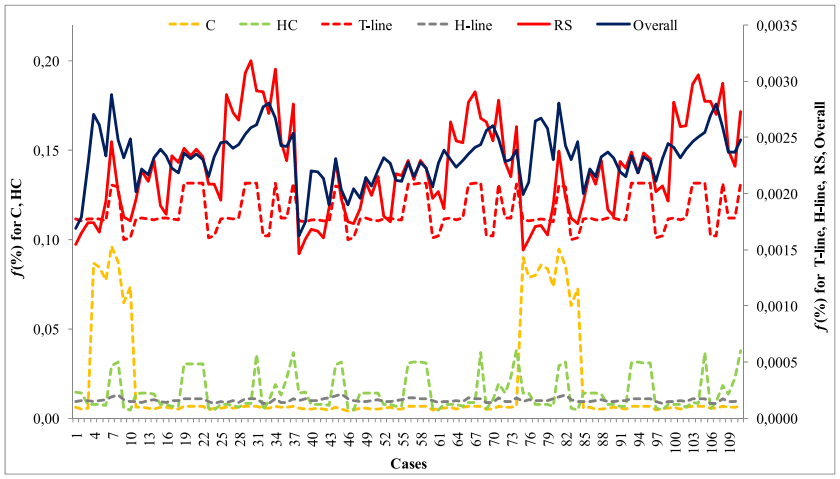


**Fig. 6.** Exergoeconomic factor on the component basis for the formed cases.

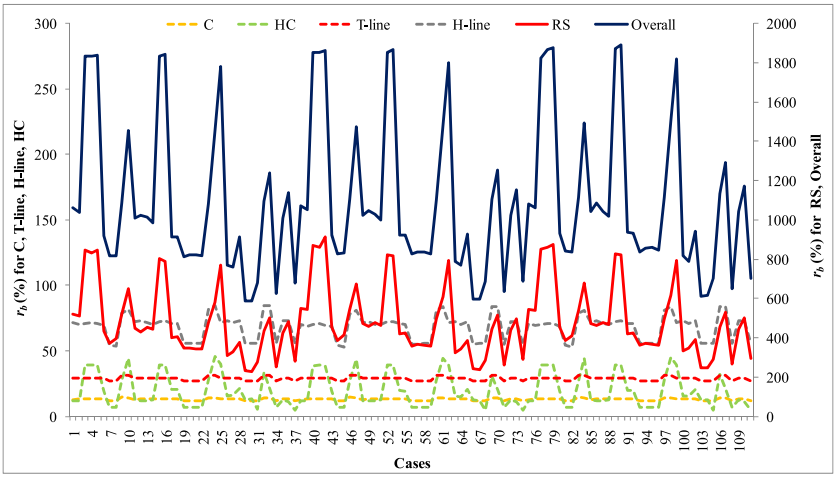


**Fig. 7.** Relative environmental impacts on the component basis for the formed cases.

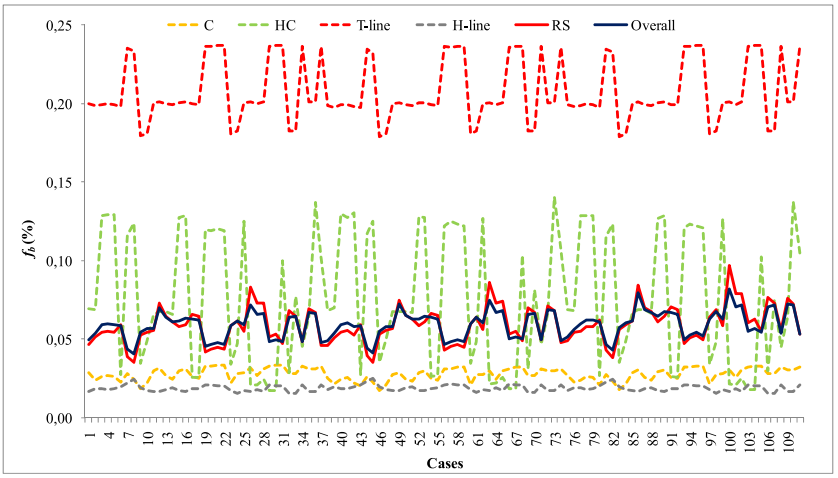


**Fig. 8.** Exergoenvironmental factor on the component basis for the formed cases.

0.095977%, 0.003884–0.006657%, and 0.004562–0.094477% for R600a, R290, and R1234ze, respectively. The exergoeconomic factor in the H-line ranges between 0.00133 and 0.000202%, 0.00135–0.000214%, and 0.00134–0.000206% for R600a, R290, and R1234ze, respectively. The exergoeconomic factor in the RS ranges between 0.001550 and 0.003180%, 0.001466–0.002909%, and 0.001497–0.003055% for R600a, R290, and R1234ze, respectively. The exergoeconomic factor in the HC ranges between 0.004296 and 0.036404%, 0.004414–0.038174%, and 0.004370–0.037482% for R600a, R290, and R1234ze, respectively. For the overall system, the exergoeconomic factor ranges between 0.001686 and 0.002880%, 0.001618–0.002606%, and 0.001995–0.002802% for R600a, R290, and R1234ze, respectively. The C and HC come into prominence as the critical components from the component-related exergoeconomic factor point of view. This is why the required heat-transfer area increases by a higher amount compared to a lower increase in exergy destruction. This increase also strongly depends on the working conditions since it determines the requirements.

According to Fig. 7, the relative environmental impact in the T-line ranges between 26.930 and 31.114%, 26.917–31.111%, and 26.924–31.113% for R600a, R290, and R1234ze, respectively. The relative environmental impact in the C ranges between 11.174 and 14.522%, 11.712–14.634%, and 11.715–14.567% for R600a, R290, and R1234ze, respectively. The relative environmental impact in the H-line ranges between 53.401 and 84.245%, 52.871–83.809%, and 53.171–84.081% for R600a, R290, and R1234ze, respectively. The relative environmental impact in the RS ranges between 228.17 and 846.07%, 239.12–912.97%, and 245.76–874.31% for R600a, R290, and R1234ze, respectively. The relative environmental impact in the HC range between 5.04 and 45.78%, 4.92–44.59%, and 4.96–45.02% for R600a, R290, and R1234ze, respectively. The overall system's relative environmental impact ranges between 585.57 and 1839.79%, 595.15–1864.42%, and 612.40–1890.55% for R600a, R290, and R1234ze, respectively. From Fig. 7, it is clearly seen that the RS system is the dominant component collimating the environmental effects.

According to Fig. 8, the exergoenvironmental factor in the T-line ranges between 0.1795 and 0.2370%, 0.1788–0.2365%, and 0.1792–0.2370% for R600a, R290, and R1234ze, respectively. The exergoenvironmental factor in the C ranges between 0.0185 and

0.0337%, 0.0172–0.0322%, and 0.0178–0.0331% for R600a, R290, and R1234ze, respectively. The exergoenvironmental factor in the H-line ranges between 0.0157 and 0.0243%, 0.0159–0.0254%, and 0.0158–0.0248% for R600a, R290, and R1234ze, respectively. The exergoenvironmental factor in the RS ranges between 0.0353 and 0.0832%, 0.0356–0.0864%, and 0.0381–0.0967% for R600a, R290, and R1234ze, respectively. The exergoenvironmental factor in the HC ranges between 0.0174 and 0.1370%, 0.0183–0.1405%, and 0.0177–0.1377% for R600a, R290, and R1234ze, respectively. For the overall system, the exergoenvironmental factor ranges between 0.0407 and 0.0717%, 0.0410–0.0748%, and 0.0432–0.0820% for R600a, R290, and R1234ze, respectively. Since all the exergoenvironmental factors are lower than 0.3 [27], the environmental impact related to the exergy destruction of the system is highly dominant. Thus, the working parameters of the system should be handled for an optimal solution.

Although geothermal energy is renewable, it has limited use depending on the reservoir conditions. So, the sustainability of the resources should be considered in the system designs. In this regard, the sustainability indexes for the formed cases were determined as given in Fig. 9. According to Fig. 9, the sustainability index ranges between 1.087 and 1.255%, 1.085–1.254%, and 1.087–1.255% for R600a, R290, and R1234ze, respectively. The best sustainability index is obtained for R600a (Case 30).

According to the exergoenvironmental and exergoeconomic analysis, the results differ for the best design, making the decision difficult. In this aim, EATWOS is a helpful tool for determining the best output from the viewpoint of multiple inlets and outlets. In the study, input and output parameters were considered to have an equal significance level. According to the results of EATWOS, as given in Fig. 10, the efficiency values change between 0.927 and 0.971. The most ineffective case was found as Case 38 with R290, whereas the most efficient case was found as Case 108 with R1234ze.

In this case, the exergy efficiency was calculated as 19.17% with a relative cost of 460.85%, a relative environmental impact of 649.50%, an exergoeconomic factor of 0.0026%, and exergoenvironmental factor of 0.0540%. The common findings are in good agreement with those of Ref. [34]. The optimized values show that it is possible to improve the system from an exergetic, economic and environmental point of view by designing the system's operating parameters with a domestic HP.

The minimum logarithmic mean temperature difference related to TES ($\Delta T_{lm}$) is recorded as 6.4 °C. The PCM is RT70HC with a melting temperature of 70 °C. The temperatures of $T_1$, $T_3$, $T_6$, $T_8$, $T_9$, $T_{10}$, $T_{11}$, $T_{12}$, and $T_{13}$ were determined as 110 °C, 50 °C, 75 °C, 55 °C, 72.94 °C, 55 °C, 35 °C, 80.47 °C, and 65 °C, respectively. $P_a$ and $P_d$ are 667.56 kPa and 1130.70 kPa, respectively. For the optimal design, the energy and exergy analysis results are given in Table 15, and the exergoeconomic and exergoenvironmental analysis results are shown in Table 16.

As seen from Table 15, the highest exergy destructions were observed in the H-line and RS since the higher power requirement, and heat losses are required. The COP of the HP system was determined as 11.71, whereas the exergy efficiency of the RS was determined as 36.75%. For the overall system, the exergetic efficiency was calculated as 19.17%, whereas the energy efficiency was determined as 74.76%.

According to Table 16, the highest component-related environmental impact of 48.43 mPts/s and stream-related environmental impact of 86622.62 mPts/s belong to RS. The highest investment cost of 0.57987 $/s and exergy cost of 19444.55 $/h also belong to RS. The relative exergoeconomic cost was 460.85%, whereas the relative exergoenvironmental impact was 649.50%. The exergoeconomic factor was determined as 0.0026%, whereas the exergoenvironmental impact was determined as 0.0540%. The exergoeconomic and exergoenvironmental analyses were also conducted to compare the proposed system with the conventional system without TES. The results are given in Table 17.

According to Table 17, the highest component-related environmental impact of 4.30 mPts/s belongs to H-line, whereas the highest stream-related environmental impact with 47765.34 mPts/s belongs to RS. The highest investment cost of 0.03237 $/s belongs to HC, whereas the highest exergy cost of 10867.4 $/h belongs to RS. The relative exergoeconomic cost was 753.70%, whereas the relative exergoenvironmental impact was 803.95%. The exergoeconomic factor was determined as 0.0003%, whereas the exergoenvironmental factor was determined as 0.0076%. The results show that the relative exergoeconomic cost and relative exergoenvironmental

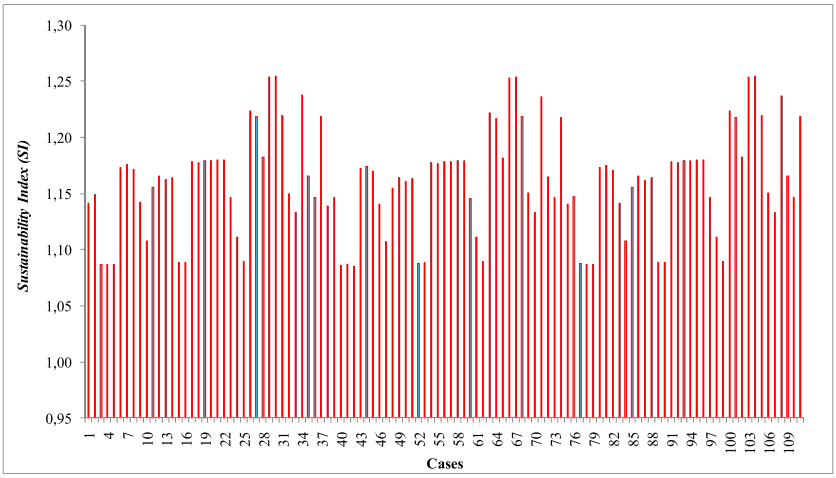


**Fig. 9.** Sustainability indexes of the formed cases.

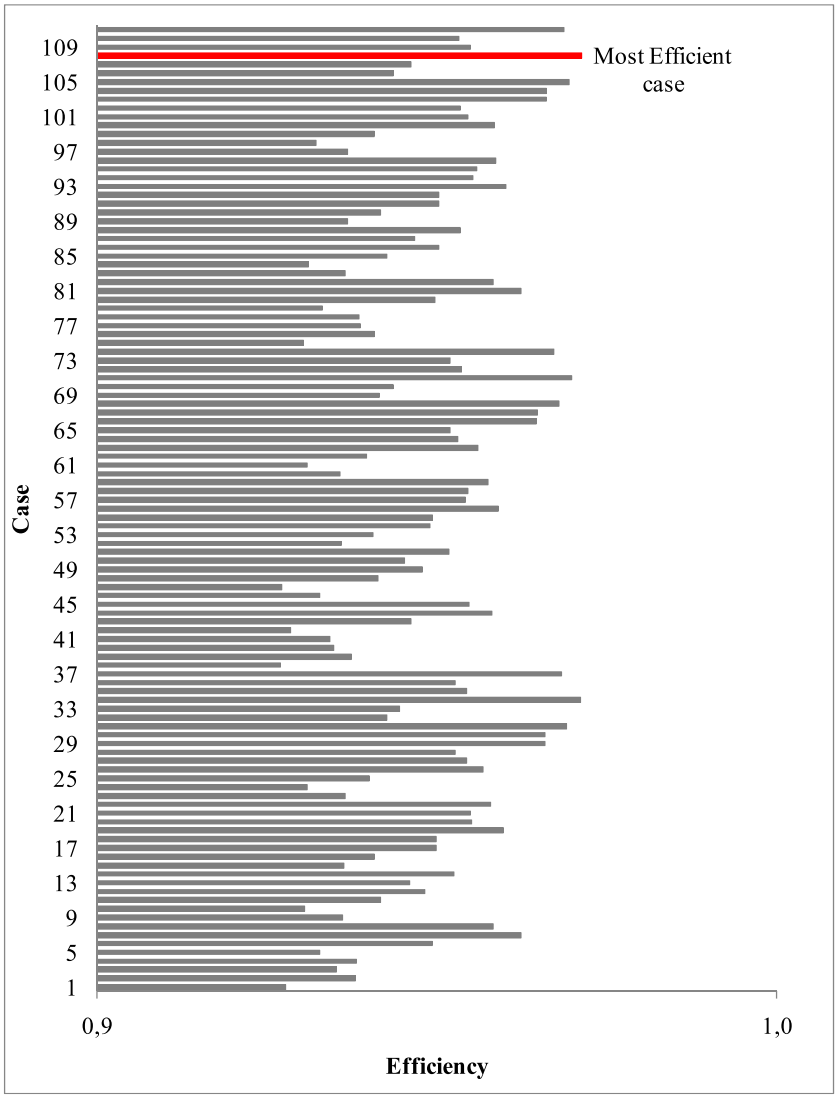


**Fig. 10.** Multi-criteria decision-making analysis outputs.

**Table 15**
Energy and exergy analysis results of optimal GDHS.

| Components | $\dot{W}$ (kW) | $\dot{Q}$ (kW) | $\dot{E}_i$ (kW) | $\dot{E}_o$ (kW) | $\dot{E}x_f$ (kW) | $\dot{E}x_p$ (kW) | $\dot{E}x_d$ (kW) | $\eta$ (%) | $\varepsilon$ (%) |
|---|---|---|---|---|---|---|---|---|---|
| T- line | 1535.00 | −1781.99 | 213178.30 | 212931.30 | 21455.47 | 19865.15 | 1590.33 | 99.17 | 92.59 |
| C | | −1145.72 | 57285.92 | 56140.20 | 10942.26 | 10050.64 | 891.62 | 98.00 | 91.85 |
| H- line | 11035.72 | −11329.47 | 335879.88 | 335586.13 | 35180.20 | 24108.30 | 11071.90 | 96.73 | 68.53 |
| RS | 4902.93 | −4619.38 | 55846.45 | 56130.00 | 14930.22 | 5486.73 | 9443.49 | 11.71[a] | 36.75 |
| HC | 70.81 | −56200.81 | 131048.11 | 74918.11 | 5781.91 | 5517.09 | 264.82 | 99.87 | 95.42 |
| **Overall system** | ***17544.4555*** | ***−18947.37*** | ***57532.91*** | ***56130.00*** | ***28779.25*** | ***5517.09*** | ***23262.16*** | ***74.76*** | ***19.17*** |

[a] COP value.

impact values increase. In contrast, exergoeconomic and exergoenvironmental factors decrease since the operating-related conditions have a more substantial effect than the component-related conditions.

## 4. Conclusions and future work

The optimization of a new GDHS integrated with a heat pump driven by a thermal energy storage unit was conducted in this study. The GDHS was investigated from the energy, exergy, economics, and environmental points of view. One hundred eleven cases were

**Table 16**
Exergoeconomic and exergoenvironmental analysis results of optimal GDHS.

| Components | $\dot{Y}_K$ (mPts/s) | $b_{f.k}$ (mPts/MJ) | $b_{p.k}$ (mPts/MJ) | $\dot{B}_{d.k}$ (mPts/s) | $\dot{B}_{total.k}$ (mPt/s) | $f_b$ (%) | $r_b$ (%) |
|---|---|---|---|---|---|---|---|
| T- line | 4.91 | 1.30 | 1.65 | 2070.66 | 2075.57 | 0.2364 | 26.98 |
| C | 0.24 | 0.83 | 0.92 | 737.07 | 737.30 | 0.0320 | 11.71 |
| H- line | 8.03 | 3.48 | 5.40 | 38477.00 | 38485.04 | 0.0209 | 55.51 |
| RS | 48.43 | 9.17 | 33.79 | 86622.62 | 86671.05 | 0.0559 | 268.35 |
| HC | 0.60 | 5.05 | 5.40 | 1337.19 | 1337.79 | 0.0446 | 6.94 |
| **Overall system** | ***62.21*** | ***4.95*** | ***37.09*** | ***115109.06*** | ***115171.27*** | ***0.0540*** | ***649.50*** |
| **Components** | $Z_K$ **($/s)** | $c_{f.k}$ **($/MJ)** | $c_{p.k}$ **($/MJ)** | $\dot{c}_{d.k}$ **($/h)** | $\dot{c}_{total.k}$ **($/h)** | $f$ **(%)** | $r$ **(%)** |
| T- line | 0.00868 | 0.07 | 0.08 | 415.37 | 415.38 | 0.0021 | 8.61 |
| C | 0.00838 | 0.04 | 0.04 | 126.46 | 126.47 | 0.0066 | 10.99 |
| H- line | 0.01643 | 0.23 | 0.34 | 9342.43 | 9342.45 | 0.0002 | 46.22 |
| RS | 0.57987 | 0.57 | 1.66 | 19444.55 | 19445.13 | 0.0030 | 190.59 |
| HC | 0.06052 | 0.34 | 0.37 | 327.85 | 327.91 | 0.0185 | 7.99 |
| **Overall system** | ***0.67387*** | ***0.31*** | ***1.75*** | ***26086.00*** | ***26086.67*** | ***0.0026*** | ***460.85*** |

**Table 17**
Exergoeconomic and exergoenvironmental analysis results of conventional GDHS.

| Components | $\dot{Y}_K$ (mPts/s) | $b_{f.k}$ (mPts/MJ) | $b_{p.k}$ (mPts/MJ) | $\dot{B}_{d.k}$ (mPts/s) | $\dot{B}_{total.k}$ (mPt/s) | $f_b$ (%) | $r_b$ (%) |
|---|---|---|---|---|---|---|---|
| T- line | 2.63 | 1.19 | 1.42 | 1882.24 | 1884.87 | 0.1393 | 19.07 |
| C | 0.16 | 0.71 | 0.78 | 611.26 | 611.41 | 0.0254 | 10.50 |
| H- line | 4.30 | 3.61 | 5.53 | 43131.07 | 43135.36 | 0.0100 | 53.04 |
| RS | 0.03 | 9.88 | 18.56 | 47565.34 | 47565.37 | 0.0001 | 87.79 |
| HC | 0.32 | 2.69 | 2.89 | 802.29 | 802.61 | 0.0398 | 7.57 |
| **Overall system** | ***7.43*** | ***4.45*** | ***40.21*** | ***98115.50*** | ***98122.94*** | ***0.0076*** | ***803.95*** |
| **Components** | $Z_K$ **($/s)** | $c_{f.k}$ **($/MJ)** | $c_{p.k}$ **($/MJ)** | $\dot{c}_{d.k}$ **($/h)** | $\dot{c}_{total.k}$ **($/h)** | $f$ **(%)** | $r$ **(%)** |
| T- line | 0.00464 | 0.07 | 0.08 | 409.87 | 409.87 | 0.0011 | 8.29 |
| C | 0.00509 | 0.04 | 0.04 | 121.05 | 121.06 | 0.0042 | 9.63 |
| H- line | 0.00879 | 0.24 | 0.36 | 10454.17 | 10454.18 | 0.0001 | 48.38 |
| RS | 0.00116 | 0.63 | 1.18 | 10867.40 | 10867.40 | 0.0000 | 87.77 |
| HC | 0.03237 | 0.18 | 0.20 | 196.71 | 196.74 | 0.0165 | 8.62 |
| **Overall system** | ***0.05205*** | ***0.28*** | ***2.37*** | ***19487.65*** | ***19487.71*** | ***0.0003*** | ***753.70*** |

formed to investigate the new system considering different working parameters. Three different working fluids, namely R600a (dry type), R290 (wet type), and R1234ze (isentropic type), were handled. The combined effects of exergy, energy, and environmental effects were considered in the optimization. Thus, exergoeconomic and exergoenvironmental indicators were used as objective functions in the multi-criteria decision-making analysis. The sustainability index was also included in the analysis for the effective use of the geothermal reservoir. The following findings were concluded:

- The exergoeconomic factors ($f$) and exergoenvironmental factors ($f_b$) are affected on a large scale by the temperature differences of the H-line fluid between the residential substation (RS) inlet and outlet ($T_5$-$T_6$) as well as the temperature differences of the HP refrigerant between the condenser (RS) inlet and outlet ($T_8$-$T_{11}$). The related factor decrease with the increase in the temperature difference.
- The relative cost ($r$) and relative environmental impact ($r_b$) are affected by the temperature difference of the HC fluid between the inlet and outlet ($T_{12}$-$T_{13}$), the temperature differences of the HP refrigerant between the condenser (RS) inlet and outlet ($T_8$-$T_{11}$). The related factor decrease with the decrease in the temperature difference.
- According to EATWOS results based on exergoeconomic and exergoenvironmental indicators, Case 108 was determined as the optimal solution case. The isentropic type (R1234ze) working fluid was found to be the most appropriate one for the TES-driven heat pump system. In this case, the GDHS inlet temperature of the geothermal source ($T_1$) is 110 °C. In this case, the system's energy efficiency is 74.56%, while the exergy efficiency is 19.17%. The COP of the TES-driven HP was determined as 11.64, which means a considerable value from the application point of view.
- For the optimal case, the environmental impact rate of exergy destruction ($\dot{B}_d = 115109.06$ mPts/s) was relatively higher than the conventional GDHS in the literature. This issue is mainly sourced by the higher electricity consumption of HP. This value will incredibly decrease if the required energy is supplied from an integrated power cycle.
- The exergoenvironmental factor of the overall system was determined to be 0.0540%. Thus, the integration of the system has an ignorable effect on the environment from the component point of view. The exergoeconomic factor of the overall system was determined to be 0.0026%. Thus, component-related exergy costs are also ignorable. However, the design parameters should be carefully selected as aimed in this study.

- When the EATWOS is driven for the single output of the selected parameters, Case 31 is the most efficient one from the sustainability of geothermal sources. In this case, the working fluid is R600a, *and* $T_1$ is 110 °C. Case 7 is the most efficient one from the exergoeconomic factor point of view. In this case, the working fluid is R600a, *and* $T_1$ is 110 °C. Case 86 is the most efficient one from the exergoenvironmental factor point of view. In this case, the working fluid is R1234ze, and $T_1$ is 100 °C.

In the study, the conducted designs were formed using geothermal energy after a power generation process. Three different temperature scales (95 °C, 100 °C, and 110 °C) were handled in this aim. Since the proposed system extremely includes power consumption, it would be more attractive to conduct the exergoeconomic and exergoenvironmental analysis for an integrated system including a power cycle as a future work.

## Credit author statement

Oguz Arslan:Analysis, Conceptualization, Methodology, Validation, Writing- Reviewing and Editing, Investigation.
Aslı Ergenekon Arslan: Data curation, EATWOS analysis, Investigation, Writing.
Irfan Kurtbas: Analysis, Methodology, Validation.

## Declaration of competing interest

The authors declare that they have no known competing financial interests or personal relationships that could have appeared to influence the work reported in this paper.

## Data availability

No data was used for the research described in the article.

## Nomenclature

$A$ area ($m^2$)
$b$ specific environmental impact (mPts/MJ)
$\dot{B}$ stream-related environmental impact (mPts/s)
$c$ unit cost of exergy flow ($/MJ)
$\dot{C}$ exergy cost rate ($/h)
$C_p$ Specific heat (kJ/kgK)
$D$ diameter (m)
$E$ multi-criteria efficiency
$\dot{E}$energy rate (kW)$\dot{Ex}$exergy rate (kW)$f$ energy rate (kW)$\dot{Ex}$exergy rate (kW)$f$exergoeconomic factor (%)
$f_b$ exergoenvironmental factor (%)
$F$ enforced convection boiling factor or correction factor
$G$ mass velocity
$Gr$ Grashof number
$h$convective heat transfer coefficient ($W/m^2K$) or specific enthalpy (kJ/kg)$ip$ convective heat transfer coefficient ($W/m^2K$) or specific enthalpy (kJ/kg)$ip$distance matrices for input ($kg/m^2s$)
$J$ dimensionless heat factor
$k$ conductive heat transfer coefficient (W/mK)
$\dot{m}$mass flow rate (kg/s)$n$ mass flow rate (kg/s)$n$number of plate or pipe
$Nu$ Nusselt number
$op$ distance matrices for output
$P$pressure (kPa, bar or atm)$Pr$ pressure (kPa, bar or atm)$Pr$Prandtl number
$\dot{q}$ heat rate per length (kW/m)
$\dot{Q}$heat rate (kW)$r$radius (m), relative cost (%) or normalized output$r_b$ heat rate (kW)$r$radius (m), relative cost (%) or normalized output$r_b$relative environmental impact (%)
$Re$ Reynolds number
$s$specific entropy (kW/kgK) or normalized input$S$ specific entropy (kW/kgK) or normalized input$S$effectiveness factor
$SI$ sustainability index
$T$temperature (K or $^oC$)$U$ temperature (K or $^oC$)$U$Total heat transfer coefficient ($W/m^2K$)
$v$ weight for output
$V$ volume ($m^3$)
$w$ weight for input
$\dot{W}$work rate (kW)$x$ work rate (kW)$x$input value, dryness fraction
$y$ output value
$\dot{Y}$ component-related environmental impact

$\dot{Z}$ investment cost

*Greek symbols*

$\beta$ volumetric expansion coefficient (−)
$\varepsilon$exergy efficiency (%)$\eta$ exergy efficiency (%)$\eta$energy efficiency (%)
$\lambda$ friction factor
$\mu$ dynamic viscosity (Ns/m$^2$)
$\nu$ Specific volume (m$^3$/kg)
$\rho$ density (kg/m$^3$)
$\sigma$ surface tension (N/m)

*$\psi$specific flow exergy (kJ/kg)Subscripts*

*b* boiling
*d* destruction
*e* enforced convective, electricity saving
*f* fluid phase, heat saving
*fg* fluid-gas mixture phase
*g* gas phase
*h* hydraulic
*i* inner, inlet, or ith component
*if* two-phase condition
*ins* insulation
*k* kth component
*lm* logarithmic mean
*m* melting
*o* outer, outlet
*Q* heat-related terms
*T* value at a specified temperature
*w* wall conditions
*W* work-related terms
0 value at the reference state

*Superscripts*

* normalized values

*Abbreviations*

C Heat center
Con Condenser
Comp Compressor
COP Coefficient of performance
DHS District heating system
Eva Evaporator
GDHS Geothermal district heating system
GWP Global warming potential
HC Heating circuit
HEx Heat exchanger
H-line Heating zone transmission line
HP Heat pump
MCDM Multi-criteria decision making
NPV Net present value
ODP Ozone depletion potential
PCM Phase change material
PR Panel radiator
RS Residential substation
T-line Geothermal zone transmission line
TES Thermal energy storage
V Extension valve

## References


[1] J.W. Lund, G.W. Huttrer, A.N. Toth, Characteristics and trends in geothermal development and use, 1995 to 2020, Geothermics 105 (2022), 102522.
[2] Arslan O, Ozgur MA, Kose R. Electricity generation ability of the Simav geothermal field: a technoeconomic approach. Energy Sources, Part A Recovery, Util. Environ. Eff. 34:12. 1130-1144.
[3] A. Tugcu, O. Arslan, R. Kose, N. Yamankaradeniz, Thermodynamics and economical analysis of geothermal assisted absorption refrigeration system: Simav case study, J Turkish Soc Thermal Sci Technol 36 (2016) 143–159.
[4] O. Arslan, R. Kose, Exergoeconomic optimization of integrated geothermal system in Simav. Kutahya, Energy Convers. Manag. 51 (2010) 663–676.
[5] J.W. Lund, A.N. Toth, Direct utilization of geothermal energy 2020 worldwide review, Geothermics 90 (2021), 101915.
[6] L. Ozgener, A. Hepbasli, I. Dincer, Exergy analysis of two geothermal district heating systems for building applications, Energy Convers. Manag. 48 (2007) 1185–1192.
[7] A. Keçebaş, M. Kayfeci, E. Gedik, Performance investigation of the Afyon geothermal district heating system for building applications: exergy analysis, Appl. Therm. Eng. 31 (2011) 1229–1237.
[8] H. Yazici, Energy and exergy based evaluation of the renovated Afyon geothermal district heating system, Energy Build. 127 (2016) 794–804.
[9] O. Arslan, M.A. Ozgur, R. Kose, A. Tugcu, Exergoeconomic evaluation on the optimum heating circuit system of Simav geothermal district heating system, Energy Build. 41 (2009) 1325–1333.
[10] O. Arslan, A.E. Arslan, Pareto principle-based advanced exergetic evaluation of geothermal district heating system: Simav case study, J. Build. Eng. 58 (2022), 105035.
[11] W. Ying, Z. Yufeng, Analysis of the dilatancy technology of district heating system with high-temperature heat pump, Energy Build. 47 (2012) 230–236.
[12] Z. Qunli, C. Mingkai, Z. Qiuyue, D. Hongfa, Research on a new district heating method combined with hot water driven ground source absorption heat pump, Energy Proc. 75 (2015) 1242–1248.
[13] Galantino CR, Beyers S, Anderson CL. Tester JW. Optimizing Cornell's future geothermal district heating performance through systems engineering and simulation. Energy Build. 201; 230: 110529.
[14] X. Zhang, Numerical study of geothermal district heating from a ground heat exchanger coupled with a heat pump system, Appl. Therm. Eng. 185 (2021), 116335.
[15] F. Sun, B. Hao, L. Fu, H. Wu, Y. Xie, H. Wu, New medium-low temperature hydrothermal geothermal district heating system based on distributed electric compression heat pumps and a centralized absorption heat transformer, Energy 232 (2021), 120974.
[16] H. Arat, O. Arslan, Exergoeconomic analysis of district heating system boosted by the geothermal heat pump, Energy 119 (2017) 1159–1170.
[17] H. Arat, O. Arslan, Optimization of district heating system aided by geothermal heat pump: a novel multistage with multilevel ANN modelling, Appl. Therm. Eng. 111 (2017) 608–623.
[18] Z. He, A.S. Farooq, W. Guo, P. Zhang, Optimization of the solar space heating system with thermal energy storage using data-driven approach, Renew. Energy 190 (2022) 764–777.
[19] D. Matuszewska, M. Kuta, P. Olczak, Techno-economic assessment of mobilized thermal energy storage system using geothermal source in Polish conditions, Energies 13 (2020) 3404.
[20] B. Rezaie, B.V. Reddy, M.A. Rosen, Exergy analysis of thermal energy storage in a district energy application, Renew. Energy 74 (2015) 848–854.
[21] G. Manente, A. Lazzaretto, I. Molinari, F. Bronzini, Optimization of the hydraulic performance and integration of a heat storage in the geothermal and waste-to-energy district heating system of Ferrara, J. Clean. Prod. 230 (2019) 869–887.
[22] O. Arslan, A.E. Arslan, Performance evaluation and multi-criteria decision analysis of thermal energy storage integrated geothermal district heating system, Process Saf. Environ. Protect. 167 (2022) 21–33.
[23] S.A. Kyriakis, P.L. Younger, Towards the increased utilization of geothermal energy in a district heating network through the use of a heat storage, Appl. Therm. Eng. 94 (2016) 99–110.
[24] D. Kim, D. Lee, J. Heo, M. Kim, Empirical results and operational cost analysis of geothermal heat pump system using thermal energy storage in cooling season, Korean Journal of Air-Conditioning and Refrigeration Engineering 30 (2018) 167–174.
[25] H. Hemmatabady, B. Welsch, J. Formhals, I. Sass, AI-based enviro-economic optimization of solar-coupled and standalone geothermal systems for heating and cooling, Appl. Energy 311 (2022), 118652.
[26] S. Siddiqui, J. Macadam, M. Barrett, The operation of district heating with heat pumps and thermal energy storage in a zero-emission scenario, Energy Rep. 7 (2021) 176–183.
[27] L.A. de Araujo Passos, P. van den Engel, S. Baldi, B. De Schutter, Dynamic optimization for minimal HVAC demand with latent heat storage, heat recovery, natural ventilation, and solar shadings, Energy Convers. Manag. 276 (2023), 116573.
[28] O. Arslan, A.E. Arslan, T.E. Boukelia, Modelling and optimization of domestic thermal energy storage based heat pump system for geothermal district heating, Energy Build. 282 (2023), 112792.
[29] L. Meyer, G. Tsatsaronis, J. Buchgeister, L. Schebek, Exergoenvironmental analysis for evaluation of the environmental impact of energy conversion systems, Energy 34 (2009) 75–89.
[30] A.S. Mousavi, M. Mehrpooya, A comprehensive exergy-based evaluation on cascade absorption-compression refrigeration system for low temperature applications-exergy, exergoeconomic, and exergoenvironmental assessments, J. Clean. Prod. 246 (2020), 119005.
[31] F. Zhang, Y. Yan, G. Liao, E. Jiaqiang, Energy, exergy, exergoeconomic and exergoenvironmental analysis on a novel parallel double-effect absorption power cycle driven by the geothermal resource, Energy Convers. Manag. 258 (2022), 115473.
[32] E.J.C. Cavalcanti, Exergoeconomic and exergoenvironmental analyses of an integrated solar combined cycle system, Renew. Sustain. Energy Rev. 67 (2017) 507–519.
[33] A. Kecebas, A. Hepbasli, Conventional and advanced exergoeconomic analyses of geothermal district heating systems, Energy Build. 69 (2014) 434–441.
[34] P. Kecebas, H. Gokgedik, M.A. Alkan, A. Kecebas, An economic comparison and evaluation of two geothermal district heating systems for advanced exergoeconomic analysis, Energy Convers. Manag. 84 (2014) 471–480.
[35] A. Kecebas, Exergoenvironmental analysis for a geothermal district heating system: an application, Energy 94 (2016) 391–400.
[36] M. Yurusoy, A. Kecebas, Advanced exergo-environmental analyses and assessments of a real district heating system with geothermal energy, Appl. Therm. Eng. 113 (2017) 449–459.
[37] O. Arslan, Ultimate Evaluation of Simav-Eynal Geothermal Resources: Design of Integrated System and its Energy-Exergy Analysis, Ph.D. Thesis, Eskisehir Osmangazi University. Institute of Applied Sciences, 2008.
[38] TSE (Turkish Standards Institution), TS 825: Thermal Insulation Requirements for Buildings, May 2008.
[39] O. Arslan, M.A. Ozgur, H.D. Yildizay, R. Kose, Fuel effects on optimum insulation thickness: an exergitic approach, Energy Sources, Part A: Recovery, Utilization, and Environmental Effects 2009 32 (2009) 128–147.
[40] REFPROP, Reference Fluid Thermodynamics and Transport Properties. NIST Reference Database. Version 9.0, National Institute of Standards and Technology. NIST, USA, 2010.
[41] DARMENT, Properties of R290, 2023. https://darment.eu/refrigerant/r290/. (Accessed 18 December 2023).
[42] DARMENT, Properties of R600a, 2023. https://darment.eu/refrigerant/r600a/. (Accessed 18 December 2023).
[43] DARMENT, Properties of R1234ze, 2023. https://darment.eu/refrigerant/r1234ze/. (Accessed 18 December 2023).
[44] RUBITHERM, Phase change materials, Available from: https://www.rubitherm.eu/en/index.php/productcategory/organische-pcm-rt. (Accessed 7 April 2022).
[45] M. Tenpierik, Y. Wattez, M. Turrin, T. Cosmatu, S. Tsafou, Temperature control in (translucent) phase change materials applied in facades: a numerical study, Energies 12 (2019) 3286.
[46] H. Yuncu, S. Kakac, Basic Heat Transfer, Bilim Publishing, Ankara, 1999 (in Turkish).

[47] J.S. Lim, A. Bejan, The Prandtl number effect on melting dominated by natural convection, ASME Journal Heat Transfer 114 (1992) 784–787.
[48] Y. Wu, D. Li, W. Jiang, S. Zhu, X. Zhao, M. Arici, E. Tuncbilek, Energy storage and exergy efficiency of a shell and tube latent thermal energy storage unit with non-uniform length and distributed fins, Sustain. Energy Technol. Assessments 53 (2022), 102362.
[49] M.R. Mohaghegh, S.H. Tasnim, S. Mahmud, A geometrical optimization and comparison study on the charging and discharging performance of shell-and-tube thermal energy storage systems, J. Energy Storage 51 (2022), 104549.
[50] O.F. Genceli, Heat Exchangers, Birsen Publication, Istanbul, 1999 (in Turkish).
[51] S. Kakac, H. Liu, A. Pramuanjaroenkij, Heat Exchangers Selection. Rating and Thermal Design, 3th edition, CRC Press. Taylor and Francis Group, Florida, 2012.
[52] O. Kizilkan, Investigation of the effects of the baffles on the heat transfer coefficient and pressure drop in a shell and tube heat exchanger, Suleyman Demirel Univ. J. Nat. Appl. Sci. 11 (2009) 246–251.
[53] Jiangyin M&C Heat Parts, NT250L type heat exchangers, Available from, https://turkish.heat-exchangergasket.com/sale-14362173-titanium-0-5mm-nt250l-plate-heat-exchanger-plate-for-sea-water-fluid.html, 2022. (Accessed 15 October 2022).
[54] R. Selbas, O. Kizilkan, M. Reppich, A new design approach for shell-and-tube heat exchangers using genetic algorithms from economic point of view, Chem. Eng. Process 45 (2006) 268–275.
[55] Y.A. Cengel, J.M. Boles, Fluid Mechanics: Fundamentals and Applications, fourth ed., McGraw Hill, New York, 2018.
[56] A. Bejan, G. Tsatsaronis, M.J. Moran, Thermal Design and Optimization, John Wiley and Sons, New York, 1996.
[57] Y. Liu, J. Han, H. You, Exergoeconomic analysis and multi-objective optimization of a CCHP system based on LNG cold energy utilization and flue gas waste heat recovery with CO2 capture, Energy 190 (2020), 116201.
[58] CBRT (Central Bank of Republic of Turkey), Inflation report, Available from, https://www.tcmb.gov.tr/wps/wcm/connect/EN/TCMB+EN/Main+Menu/Core+Functions/Monetary+Policy/Rediscount+and+Advance+Interest+Rates, 2022. (Accessed 7 December 2022).
[59] Towering skills. Cost indices, Available from, https://www.toweringskills.com/financial-analysis/cost-indices/#cepci-2001-to-present. (Accessed 15 December 2022).
[60] M. Goedkoop, R. Spriensma, Amersfoort. Netherlands, in: The Eco-Indicator 99: A Damage Oriented Method for Life Cycle Impact Assessment. Methodology Annex, third ed., 2001. Available from: https://pre-sustainability.com/legacy/download/EI99_annexe_v3.pdf.
[61] M. Weckert, Comparative Life Cycle Assessment of CFC-Replacement Compounds in Different Technical Applications, Ph.D. Dissertation, University of Bayreuth, Germany, 2008.
[62] Eco-indicator 99, Manuel for designers, 2000. Available from: https://pre-sustainability.com/legacy/download/EI99_Manual.pdf.
[63] F. Lu, Y. Zhu, M. Pan, C. Li, J. Yin, F. Huang, Thermodynamic, economic, and environmental analysis of new combined power and space cooling system for waste heat recovery in waste-to-energy plant, Energy Convers. Manag. 226 (2020), 113511.
[64] A.E. Arslan, O. Arslan, S.Y. Kandemir, AHP–TOPSIS hybrid decision-making analysis: Simav integrated system case study, J. Therm. Anal. Calorimetry 145 (2021) 1191–1202.
[65] A.E. Arslan, M.S. Acar, O. Arslan, Optimization of O-type ORC-Binary geothermal power plant: EATWOS analysis, BSEU J. Sci. 6 (2019) 222–236, https://doi.org/10.35193/bseufbd.601745.
[66] O. Arslan, A.E. Arslan, M.S. Acar, Multi-criteria making-decision modeling of b-type ORC-binary geothermal power plant: EATWOS analysis, BSEU J. Sci. 6 (2019) 29–48, https://doi.org/10.35193/bseufbd.561668.
[67] M.L. Peters, S. Zelewski, Efficiency analysis under consideration of satisficing levels for output quantities, in: Proceedings of the 17th Annual Conference of the Production and Operations Management Society (POMS), April 28-May 01. 2006 (Boston. USA).